Comput. Methods Appl. Mech. Engrg. 199 (2010) 916–931

Contents lists available at ScienceDirect

Comput. Methods Appl. Mech. Engrg.

journal homepage: www.elsevier.com/locate/cma

Numerical analysis and computational comparisons of the NS-alpha and NS-omega regularizations

William Layton [a,*,1], Carolina C. Manica [b], Monika Neda [c], Leo G. Rebholz [d]

[a] Department of Mathematics, University of Pittsburgh, United States
[b] Departmento de Matemática, Universidade Federal do Rio Grande do Sul, Brazil
[c] Department of Mathematical Sciences, University of Nevada Las Vegas, United States
[d] Department of Mathematical Sciences, Clemson University, United States

ARTICLE INFO

Article history:
Received 7 January 2008
Received in revised form 5 January 2009
Accepted 12 January 2009
Available online 23 January 2009

Keywords:
NS-α model
Finite element method
Large Eddy simulation

ABSTRACT

We study stability, accuracy and efficiency of algorithms for a new regularization of the NSE, the NS-$\bar{\omega}$ model (in which the vorticity term, $\bar{\omega} = \nabla \times \bar{u}$, is averaged) given by

$$u_t - u \times (\nabla \times \bar{u}) + \nabla q - \nu \Delta u = f, \quad \nabla \cdot u = 0.$$

This is similar to the NS-α model (in which the nonlinear term is $\bar{u} \times (\nabla \times u)$), but the small difference opens attractive algorithmic possibilities. We give tests both confirming the predicted rates of convergence and exhibiting some shared limitations of both models. The experiments also show the discrete NS-$\bar{\omega}$ simulation has *greater accuracy* (Tables 3 and 4) at *less cost* (Table 2) and requires significantly *fewer* degrees of freedom (Section 1.1) than a comparable NS-α simulation. The experiments suggest consideration of adding grad–div stabilization and higher accuracy NS-$\bar{\omega}$-deconvolution models as a next logical step. In fact, this combination produced accurate results (see Figs. 10 and 11) on the coarsest mesh (mesh 1) upon which all other methods, models and variants tested failed.

© 2009 Elsevier B.V. All rights reserved.

1. Introduction

This report presents a numerical analysis and computational testing of a (to our limited knowledge) new regularization of the Navier–Stokes equations (NSE) that we call the NS-omega (NS-$\bar{\omega}$) model of turbulent flow. The regularization (1.1)–(1.3) below is motivated by a desire for efficient, accurate, and reliable under-resolved simulations of flow problems and has evolved from our work on algorithms for, e.g., the NS-α model, the rational model and deconvolution models. The NS-$\bar{\omega}$ model is derived from the rotational form of the NSE by filtering, with the differential filter/rational filter/Helmholtz filter, the second term of the nonlinearity (for reasons explained below)

$$u_t - u \times (\nabla \times \bar{u}) + \nabla q - \nu \Delta u = f, \tag{1.1}$$
$$\nabla \cdot u = 0, \tag{1.2}$$
$$-\alpha^2 \Delta \bar{u} + \bar{u} = u. \tag{1.3}$$

NS-$\bar{\omega}$ is a complement to the NS-α model (1.4)–(1.6) next. The NS-α/viscous Camassa–Holm model (1.4)–(1.6) is a recently developed regularization of the NSE with desirable mathematical properties, e.g., [15,14,23]. It is given by

$$u_t - \bar{u} \times (\nabla \times u) + \nabla q - \nu \Delta u = f, \tag{1.4}$$
$$\nabla \cdot \bar{u} = 0, \tag{1.5}$$
$$-\alpha^2 \Delta \bar{u} + \bar{u} = u. \tag{1.6}$$

We consider the NS-$\bar{\omega}$ model (1.1)–(1.3) either for internal flow, i.e. for a bounded, polyhedral domain in $\mathbb{R}^d, d = 2, 3$, subject to no-slip boundary conditions, or for $\Omega = (0, L)^d$ and subject to L periodic boundary conditions with zero mean imposed on the solution and all data. A mathematical theory for the continuous NS-$\bar{\omega}$ model has also been recently developed, [40].

Comparing (1.1)–(1.3) to (1.4)–(1.6), the NS-$\bar{\omega}$ model averages the vorticity term $\omega = \nabla \times u$ rather than the velocity term in the nonlinearity. (Hence calling it the NS-$\bar{\omega}$ regularization seems descriptive.) This modification is similar in form to that of the

* Corresponding author.
E-mail addresses: wjl@pitt.edu (W. Layton), carolina.manica@ufrgs.br (C.C. Manica), Monika.Neda@unlv.edu (M. Neda), rebholz@clemson.edu (L.G. Rebholz).
URLs: http://www.math.pitt.edu/~wjl (W. Layton), http://chasqueweb.ufrgs.br/~carolina.manica (C.C. Manica), http://faculty.unlv.edu/neda (M. Neda), http://www.math.clemson.edu/~rebholz (L.G. Rebholz).
[1] Partially supported by NSF Grants DMS 0508260 and 0810385.

0045-7825/$ - see front matter © 2009 Elsevier B.V. All rights reserved.
doi:10.1016/j.cma.2009.01.011

modified Leray model, [28] but it differs in motivation and consequence.

The difference (in the non-periodic case) between the imposition of incompressibility in (1.2) and (1.5) arises from filtering the different terms in the nonlinearity in (1.1) and (1.4). The choices (1.2) and (1.5) are necessary for model stability ($\nu > 0$) and energy conservation ($\nu = 0$).

In this report, we compare variants of Crank–Nicolson (CN) finite element method (FEM) algorithms for NS-$\bar{\omega}$ and NS-α. In Section 3, we study CN algorithms for both models (necessary notation and preliminaries are presented in Section 2). We give a numerical analysis for the CN scheme for NS-$\bar{\omega}$ that includes proofs of unconditional stability and solvability, as well as convergence. Analysis of the CN scheme for NS-α was performed in [11] and in [8] for a reformulated method. We also study a second order, unconditionally stable, linearly implicit variant (CNLE) of CN for NS-$\bar{\omega}$. In Section 4, we present numerical experiments for the schemes. Here we confirm predicted convergence rates, and compare runtimes and errors for the CN schemes for both NS-α and NS-$\bar{\omega}$. We also consider linearly and quadratically extrapolated CN schemes for NS-$\overline{\omega}$; we discuss in Section 3 why such linearizations lose their strong unconditional stability for NS-α. In tests in Section 4, significantly better runtimes and errors are found for the NS-$\bar{\omega}$ schemes.

Lastly, we present experiments for the well-known benchmark problems of two-dimensional flow around a cylinder and flow over a step problems. It is our view that understanding the limitations of a model or algorithm is often more important than reporting yet another similar success. These test problems are difficult since they are near a critical Reynolds number *Re* for vortex shedding. Often, regularizations produce solutions which resemble lower *Re* solutions (i.e., without shedding). Although both NS-α and NS-$\bar{\omega}$ are dispersive regularizations, neither gives perfect solutions on meshes that are coarser than required for direct simulation using the Navier–Stokes equation. For the flow around a cylinder problem, NS-α simulation fails dramatically on mesh 1 and robust iterative solvers fail to converge on mesh 2 for the linear and nonlinear systems arising from the discrete NS-α model. The discretized NS-$\bar{\omega}$ system presents no difficulty to the solvers but gave a similar solution on mesh 1 to the NS-α model. The mesh 2 solution produces a vortex street configuration which is over-damped in the cylinder wake. We obtained similar results for the step problem, with neither model accurately predicting Eddy detachment.

These poor results led to more detailed tests, and we believe a better understanding of the shortcomings. The bad convergence of iterative solvers for the discrete NS-α model seems a genuine problem specific to NS-α. We conjecture that it is due to the natural energy norm for NS-α being a rather weak norm. (This restricts the predicted radius of attraction of Newton's method in the Kantorovich theory.) This effect is under study and we believe a better understanding will lead to improved solvers for NS-α. The bad results for the cylinder problem are really due to the (essential) use of the rotational forms for both models. Indeed, although the NSE as usually solved gave good results on mesh 2, the NSE in rotational form gave no better results on any mesh than either model. (In fact, NS-$\bar{\omega}$ gave marginally better results on mesh 2 than the NSE in rotational form.)

A compelling explanation for this accuracy loss (and its "fix") associated with the rotational form of the NSE is given in [35]. We thus repeated the above experiments adding the fix of the grad–div stabilization, see Fig. 5 through Fig. 11. These experiments show good results where the ones described above without it show bad ones. Indeed, on mesh 2 the NS-$\bar{\omega}$ simulation gives essentially perfect results, Fig. 5. See also Figs. 8 and 9 for the step problem without stabilization (bad results, Fig. 8) and with it (good result, Fig. 9). We also give a preliminary test of a higher accuracy NS-$\bar{\omega}$-deconvolution simulation for both problems in Figs. 10 and 11. The combination of the $N = 1$ NS-$\bar{\omega}$-deconvolution model with grad–div stabilization gave perfect results even on the coarsest mesh (mesh 1) upon which all the other variants failed, see Figs. 10 and 11.

1.1. Motivation for NS-$\bar{\omega}$

Our motivation for studying the modification (1.1)–(1.3) from (1.4)–(1.6) is the search for efficient, unconditionally stable and (at least second order) accurate methods for the simulation of under-resolved flows. The classic beginning point for such methods, studied by Caglar [8] and Connors [11] for NS-α, is a variational discretization in space plus the Crank–Nicolson method in time. Suppressing spatial discretization and letting $u^{n+1/2} := (u^{n+1} + u^n)/2$, for NS-$\alpha$ (1.4)–(1.6) it is given by

$$\frac{u^{n+1} - u^n}{\Delta t} - w^{n+\frac{1}{2}} \times (\nabla \times u^{n+\frac{1}{2}}) - \nu \Delta u^{n+\frac{1}{2}} + \nabla p^{n+\frac{1}{2}} = f^{n+\frac{1}{2}}, \tag{1.7}$$

$$\nabla \cdot w^{n+\frac{1}{2}} = 0, \tag{1.8}$$

$$-\alpha^2 \Delta w^{n+\frac{1}{2}} + w^{n+\frac{1}{2}} = u^{n+\frac{1}{2}}. \tag{1.9}$$

This is second order accurate for NS-α and nonlinearly, unconditionally stable (take the inner product of the discrete equations with $w^{n+\frac{1}{2}}$). However, in finite element spaces with N_V velocity degrees of freedom and N_P pressure degrees of freedom, *the method leads to a large, nonlinear system at each time step with* $2N_V + N_P$ *total degrees of freedom*. There does not appear to be any method for NS-α which preserves these attractive properties and has significantly less complexity.

On the other hand, because of the structure of the nonlinearity, the NS-$\bar{\omega}$ model (1.1)–(1.3) admits simple methods which are nonlinearly, unconditionally stable, second order accurate, *linearly implicit* (only 1 linear system per time step) and require only $N_V + N_P$ total degrees of freedom. Herein we study both the full Crank–Nicolson method for NS-$\bar{\omega}$ as well as the following attractive variant CNLE (Crank–Nicolson with linear extrapolation, known for the NSE at least since Baker's 1976 paper [1]). Let $u^{n+1/2} := (u^{n+1} + u^n)/2$ and $U^n := \frac{3}{2}u^n - \frac{1}{2}u^{n-1}$

$$\frac{u^{n+1} - u^n}{\Delta t} - u^{n+\frac{1}{2}} \times (\nabla \times \overline{U^n}) - \nu \Delta u^{n+\frac{1}{2}} + \nabla p^{n+\frac{1}{2}} = f^{n+\frac{1}{2}},$$
$$\text{and} \quad \nabla \cdot u^{n+\frac{1}{2}} = 0. \tag{1.10}$$

We prove unconditional stability (take the inner product with $u^{n+\frac{1}{2}}$). It is clearly second order accurate and linearly implicit (since $U^n := \frac{3}{2}u^n - \frac{1}{2}u^{n-1}$ is known from previous time levels). Further, since $\overline{U^n} := \frac{3}{2}u^n - \frac{1}{2}u^{n-1}$ is known, its average can be directly computed, uncoupled from the linear equations for advancing in time. We also discuss the Crank–Nicolson quadratic extrapolation (CNQE) in Section 2 and give experiments for it in Section 4, where U^n is extrapolated quadratically as $U^n := \frac{15}{8}u^n - \frac{10}{8}u^{n-1} + \frac{3}{8}u^{n-2}$.

The NS-$\bar{\omega}$ regularization (1.1)–(1.3) exactly conserves (under periodic boundaries and no viscous or external forces) the two key integral invariants for three dimensional fluid flow (note $\|\cdot\|$ and $(\cdot,\cdot)$ denote the usual L^2 norm and inner product): energy, $\frac{1}{2}\|u\|^2$, and (model) helicity, $(u, \nabla \times \bar{u})$, Proposition 1.1 below. Helicity is a fundamentally important quantity in turbulent fluid flow. It is a scalar quantity describing *rotation* that is conserved by the Euler equations, cascaded through the inertial range in homogeneous, isotropic turbulence, and provides important information on the topology of vortex filaments [43]. Helicity density has been used as an indicator of coherent structures, and moreover, as an indicator of low turbulent dissipation. The Pythagorean identity gives

$$\frac{(u \cdot (\nabla \times u))^2 + |u \times (\nabla \times u)|^2}{|u|^2 |\nabla \times u|^2} = 1, \tag{1.11}$$

which can be interpreted as

$$\frac{\text{helicity}^2 + \text{nonlinearity}^2}{\text{energy} \cdot \text{enstrophy}} = 1. \tag{1.12}$$

Hence at constant energy and enstrophy, high helicity implies small nonlinearity, and conversely. The interaction between model's treatment of energy and helicity impacts its predictions of a flow's rotational structures.

Proposition 1.1. *In the absence of viscosity and external forces ($\nu = f = 0$), and for periodic boundary conditions, the NS-$\bar{\omega}$ model 1.1,1.2,1.3 conserves energy, $\frac{1}{2}\|u\|^2$, and a model helicity, $(u, \nabla \times \bar{u})$: For $t > 0$,*

$$\frac{1}{2}\|u(t)\|^2 = \frac{1}{2}\|u(0)\|^2, \tag{1.13}$$

$$(u(t), \nabla \times \overline{u(t)}) = (u(0), \nabla \times \overline{u(0)}). \tag{1.14}$$

Proof. The proof for each result begins by setting $\nu = f = 0$ in (1.1). For energy, multiply by u and integrate over Ω. The nonlinearity and pressure term vanish. This leaves only $\frac{1}{2}\frac{d}{dt}\|u\|^2 = 0$. Integrating over time gives the result. The proof for helicity requires multiplying by $\nabla \times \bar{u}$ and integrate over Ω. This leaves $(u_t, \nabla \times \bar{u}) = 0$. Integrating over time and using the fact that differential operators (including the filter) commute under periodic boundary conditions completes the proof. □

Many models and regularizations do not exactly conserve (any form of) helicity, [47], and this clearly impacts the reliability of their predictions in highly rotational flows and over longer time intervals. The nonlinearity of NS-$\bar{\omega}$ acts in manner physically consistent with true fluid flow in that it neither creates nor dissipates either energy or helicity. In homogeneous, isotropic turbulence, energy and model helicity conservation suggests that both energy and model helicity in NS-$\bar{\omega}$ cascade from large (input) scales to small scales where they are dissipated strongly by viscosity ([40], and the helicity case follows [36]). It is interesting to note that the three dimensional integral invariants for NS-$\bar{\omega}$ are, in some sense, reversed from those of NS-α. The NS-α model conserves a weaker model energy, $\frac{1}{2}(u, \bar{u})$, than NS-$\bar{\omega}$, and the usual helicity $(u, \nabla \times u)$.

1.2. Differential filters in NS-$\bar{\omega}$ and large Eddy simulation

Large Eddy simulation is concerned with approximation of local, spatial averages in under-resolved simulations of mixes of laminar, transitional and turbulent flows. Velocity averages can be defined by a projection into a finite dimensional space (e.g., a finite element velocity space) as in the Variational Multiscale Method (VMM) of Hughes and co-workers, e.g., [24,25]. Traditionally, velocity averages $\bar{u}$ in LES are defined by convolution with a given filter

$$\bar{u}(x, t; \alpha) := (g_\alpha * u)(x, t), \quad \alpha = \text{filter radius, typically } O(h).$$

On the surface, there are many choices of filter kernel $g(\cdot)$. However, if the averages are viewed as containing information of physical meaning, there are already results on acceptable filters beginning with the famous paper of Koenderink [32], see also Sagaut [48]. Scale space analysis begins with some basic postulates that any physically reasonable filter should satisfy. In [32] (see also [41] for interesting developments and applications) the following is proven.

Theorem 1.1. [32] *The only filter satisfying the following four conditions is the Gaussian filter:*

linearity : $\overline{\alpha u + \beta v} = \alpha \bar{u} + \beta \bar{v}$,

spacial invariance : $\overline{u(x - a)} = \bar{u}(x - a)$,

isotropy, for all rotations R : $\bar{u}(x) = R^* \overline{u(Rx)}$,

scale invariance or the semigroup property (no preferred size) :

if $\bar{u}(x, t) := g_\alpha * u(x, t)$ *(so* $\bar{\bar{u}} := g_\alpha * g_\alpha * u$*) then* $\bar{\bar{u}} = g_{\sqrt{2}\alpha} * u$.

Thus, there is really only one mathematical correct filter: the Gaussian. Convolution with the Gaussian is expensive so that in spite of this strong uniqueness result usually other filters are used. Koenderink's result indicates that these other filters must be assessed as approximations to the Gaussian.

Differential filters like (1.3) were proposed for large Eddy simulation by Germano [16]. The close connection of the above differential filter to the Gaussian filter can be seen various ways, [5]. For example, the Gaussian is the heat kernel. Thus, one way to compute the exact Gaussian filtered velocity $\bar{u}(x, t) = g_\alpha * u(x, t)$ is to solve the following evolution equation:

$$v_s(x, s) = \Delta v(x, s) \quad \text{for } s > 0, \quad \text{and} \quad v(x, 0) = u(x),$$

then set $\bar{u}(x, t) := v(x, s)|_{s=\alpha^2}$. Since the averaging radius α is small, α^2 is smaller still and we can reasonably approximate $v(x, \alpha^2)$ by one step of backward Euler, leading back to the differential filter (1.3).

In comparison with the Gaussian, the differential filter is only approximately scale invariant. Indeed, if we compute $\bar{\bar{u}}$ it fails the semigroup property by $O(\alpha^4)$

$$\bar{\bar{u}} = (-\alpha^2\Delta + 1)^{-1}(-\alpha^2\Delta + 1)^{-1}u = (-(\sqrt{2}\alpha)^2\Delta + 1)^{-1}u + O(\alpha^4).$$

1.3. LES versus regularization

In regularization modeling, for example Leray and NS-α, one solves a system similar to the NSE which has better qualitative properties for numerical simulation than the underlying NSE. As a consequence, the computed solution is simply a regularized approximation of the NSE solution rather than a local, spatial average of the fluid velocity. The many possible NSE regularizations can be judged based on (i) accuracy as an approximation of the NSE, and (ii) fidelity to qualitative properties of the NSE's velocity.

The first regularization is due to the seminal 1934 work of Leray

$$u_t + \bar{u} \cdot \nabla u + \nabla q - \nu\Delta u = f, \quad \text{and} \quad \nabla \cdot u = 0. \tag{1.15}$$

This is $O(\alpha^2)$ consistent with the NSE. Leray proved that a unique solution exists and converges (modulo a subsequence) as the averaging radius $\alpha_j \to 0$ [33,34]. Importantly, Leray's regularization is performed so as to neither create nor destroy kinetic energy: if $\nu = f = 0$ (and under periodic boundary conditions) Leray's model exactly conserves kinetic energy.

As noted above, the 3d Euler equations have two important integral invariants: energy $\frac{1}{2}\int_\Omega |u|^2\,dx$ and helicity $\int_\Omega u \cdot \nabla \times u\,dx$. The interplay between these two are thought to organize coherent structures in fluid motion. The step from (1.15) to NS-α is that by using Leray's idea with the NSE nonlinearity in rotational form, a regularization results which exactly conserves (in the appropriate context) both a model energy and helicity. Based on the associated á priori bounds, a Leray theory (and beyond) has been established for (1.4)–(1.6) (and as well as for the NS-$\bar{\omega}$ model in [40]).

1.4. Increasing accuracy with grad–div stabilization

The viscous term in the compressible Navier–Stokes equations contain two components: a Δu term and a $\nabla(\nabla \cdot u)$ term. Since

$\nabla \cdot u = 0$ identically, the latter vanishes in the incompressible case and is usually omitted in simulations.

However, since in numerical simulations $\nabla \cdot u^h$ is seldom exactly zero, it has recently been suggested, [44–46,35], that numerical simulations should include a discrete term $(\nabla \cdot u^h, \nabla \cdot v^h)$ coming from the component of the viscous term $\nabla(\nabla \cdot u^h)$. In this context (including a dissipative term in the discretization which exactly vanishes for the Navier–Stokes equations), inclusion is called grad–div stabilization.

The rotational form of the NS-$\bar{\omega}$ and NS-α models is of special interest for numerical simulations since it requires the fewest number of dependent variables (and thus storage). It also introduces special complications. Since

$$u \cdot \nabla u + \nabla p = -u \times (\nabla \times u) + \nabla\left(\frac{1}{2}u^2 + p\right) =: -u \times (\nabla \times u) + \nabla P \tag{1.16}$$

the dynamic pressure of the either's rotational form will contain similar boundary and interior layers to the velocity. The dynamic pressure will be significantly more complex than the usual pressure, require much finer meshes for resolution and thus have much larger errors when under-resolved. This larger pressure error is coupled through the discrete momentum equation to the velocity error and causes an increased velocity error as well.

Recent studies of the grad–div stabilization term, $(\nabla \cdot u^h, \nabla \cdot v^h)$, have shown that without its stabilization, the feedback from the error in the dynamic pressure to the velocity error grows catastrophically as the Reynolds number increases [46,35]. Adding the grad–div stabilization term eliminates the catastrophic part of the pressure–velocity coupling and allows an accurate velocity simulation without full resolution of the dynamic pressure, [35]. This term has been used in residual-based stabilizations of NSE-type equations, see [6], and it is part of a recently proposed VMS method, see [3]. Numerical experiences show that the choice of the parameter in actual computations is somewhat delicate.

Adding the grad–div term to a numerical scheme also improves the convergence of linear and nonlinear solvers, reduces the dependence of the velocity error on the viscosity, and reduces the effect of large pressure gradients on the error [45,46,35]. It is important to note that grad–div stabilization is only a "fix" for linear effects (which can have a profound impact on the accuracy of rotational form NSE simulations). When these are corrected, nonlinear effects become critical to an accurate simulation. These are addressed in the treatments of the nonlinearity in the NS-α and NS-$\bar{\omega}$ models, studied herein.

In the case of wall-bounded flows, there is a difference in the correct incompressibility condition for NS-$\bar{\omega}$ ($\nabla \cdot u = 0$) and NS-α ($\nabla \cdot \bar{u} = 0$). Thus, in the NS-$\bar{\omega}$ case, grad–div stabilization is completely clear, the same as the NSE case and a natural extension that significantly improves accuracy of simulations (Sections 4 and 5).

Grad–div stabilization for the NS-α model is less clear. With one choice, adding $(\nabla \cdot u^h, \nabla \cdot v^h)$, it imposes an extra constraint ($\nabla \cdot u = 0$ in addition to $\nabla \cdot \bar{u} = 0$) and overdetermines the model. With the other possible form, $(\nabla \cdot \bar{u}^h, \nabla \cdot v^h)$, it imposes a non-local condition that couples variables across the whole domain. Its realization for NS-alpha is unclear and thus an interesting algorithmic question for further study.

2. Notation and preliminaries

This section summarizes the notation, definitions and preliminary lemmas needed. We start by introducing the following notation. The $L^2(\Omega)$ norm and inner product will be denoted by $\|\cdot\|$ and $(\cdot,\cdot)$. Likewise, the $L^p(\Omega)$ norms and the Sobolev $W_p^k(\Omega)$ norms are denoted by $\|\cdot\|_{L^p}$ and $\|\cdot\|_{W_p^k}$, respectively. For the semi-norm in $W_p^k(\Omega)$ we use $|\cdot|_{W_p^k}$. H^k is used to represent the Sobolev space $W_2^k(\Omega)$, and $\|\cdot\|_k$ denotes the norm in H^k. For functions $v(x,t)$ defined on the entire time interval $(0,T)$, we define $(1 \leqslant m < \infty)$

$$\|v\|_{\infty,k} := \operatorname*{ess\,sup}_{0<t<T} \|v(t,\cdot)\|_k, \quad \text{and}$$

$$\|v\|_{m,k} := \left(\int_0^T \|v(t,\cdot)\|_k^m \, dt\right)^{1/m}.$$

In the discrete case we use the analogous norms:

$$|||v|||_{\infty,k} := \max_{0\leqslant n\leqslant M} \|v_n\|_k, \quad |||v_{1/2}|||_{\infty,k} := \max_{0\leqslant n\leqslant M} \|v_{n+1/2}\|_k,$$

$$|||v|||_{m,k} := \left(\sum_{n=0}^{M} \|v_n\|_k^m \Delta t\right)^{1/m}, \quad |||v_{1/2}|||_{m,k} := \left(\sum_{n=0}^{M} \|v_{n+1/2}\|_k^m \Delta t\right)^{1/m}.$$

We consider both the periodic case and the case of internal flow with no slip boundary conditions. (There is mainly only small notational differences between these two cases in the analysis.)

In the periodic case, $\Omega = (0,L)^d, d = 2,3$ and pressure and velocity spaces are, respectively,

$$Q = L_0^2(\Omega) := \{q \in L^2, \ \int_\Omega q = 0\},$$

$$X = H^1_{\#}(\Omega) := \{v \in H^1(\Omega) \cap L_0^2(\Omega) : v \text{ is } L \text{ periodic}\},$$

while in the case of internal flow Ω is a regular, bounded, polyhedral domain in $\mathbb{R}^d$ and

$$Q = L_0^2(\Omega),$$

$$X = H_0^1(\Omega) := \{v \in H^1(\Omega) : \ v|_{\partial\Omega} = 0\}.$$

We denote the dual space of X by X^*, with the norm $\|\cdot\|_*$. The space of divergence free functions is denoted

$$V := \{v \in X, (\nabla \cdot v, q) = 0 \forall q \in Q\}.$$

The velocity–pressure finite element spaces $X^h \subset X$, $Q^h \subset Q$ are assumed to be conforming and satisfy the LBB^h condition, e.g. [18]. The discretely divergence free subspace of X^h is, as usual

$$V^h = \{v^h \in X^h, (\nabla \cdot v^h, q^h) = 0 \forall q^h \in Q^h\}.$$

In addition, we make use of the following approximation properties,[7]:

$$\inf_{v\in X_h} \|u - v\| \leqslant Ch^{k+1}|u|_{k+1}, \quad u \in H^{k+1}(\Omega)^d,$$

$$\inf_{v\in X_h} \|u - v\|_1 \leqslant Ch^{k}|u|_{k+1}, \quad u \in H^{k+1}(\Omega)^d,$$

$$\inf_{r\in Q_h} \|p - r\| \leqslant Ch^{s+1}|p|_{s+1}, \quad p \in H^{s+1}(\Omega).$$

Taylor–Hood elements (see e.g. [7,18]) are one common example of such a choice for (X^h, Q^h), and are also the elements we use in our numerical experiments.

We employ a skew-symmetric trilinear form that ensures stability of the method.

Definition 2.1. Define $b : X \times X \times X \to \mathbb{R}$, by

$$b(u,v,w) := ((\nabla \times u) \times v, w).$$

We now list important estimates for the b operator necessary in Section 3.

Lemma 2.2. *For $u, v, w \in X$, or $L_\infty(\Omega)$ and $\nabla \times u \in L_\infty(\Omega)$, when indicated, the trilinear term $((\nabla \times u) \times v, w)$ satisfies*

$$|((\nabla \times u) \times v, w)| \leqslant \|\nabla \times u\| \|v\|_\infty \|w\|, \tag{2.1}$$

$$|((\nabla \times u) \times v, w)| \leqslant \|\nabla \times u\|_\infty \|v\| \|w\|, \tag{2.2}$$

$$|((\nabla \times u) \times v, w)| \leqslant C_0(\Omega) \|\nabla \times u\| \|\nabla v\| \|\nabla w\|, \tag{2.3}$$

$$|((\nabla \times u) \times v, w)| \leqslant C_0(\Omega) \|v\|^{1/2} \|\nabla v\|^{1/2} \|\nabla \times u\| \|\nabla w\|. \tag{2.4}$$

Proof. The first two estimates follow immediately from the definition of b. The proof of the other two bounds are easily adapted from the usual bounds of the nonlinearity in non-rotational form. □

Since we study discretizations of the three models, we must deal with discrete differential filters. Continuous differential filters were introduced into turbulence modeling by Germano [16,17] and used in various models and regularizations [12,9,28,20,19,21].

Definition 2.3. Continuous differential filter For $\phi \in L^2(\Omega)$ and $\alpha > 0$ fixed, denote the filtering operation on ϕ by $\bar{\phi}$, where $\bar{\phi}$ is the unique solution (in X) of

$$-\alpha^2 \Delta \bar{\phi} + \bar{\phi} = \phi. \tag{2.5}$$

We denote by $A := (-\alpha^2\Delta + I)$, so $A^{-1} v = \bar{v}$. We define next the discrete differential filter, following Manica and Kaya Merdan [42].

Definition 2.4. Discrete differential filter Given $v \in L^2(\Omega)$, for a given filtering radius $\alpha > 0$, $\bar{v}^h = A_h^{-1} v$ is the unique solution in X^h of

$$\alpha^2(\nabla \bar{v}^h, \nabla \chi) + (\bar{v}^h, \chi) = (v, \chi) \forall \chi \in X^h. \tag{2.6}$$

Definition 2.5. Define the L^2 projection $\Pi^h : L^2(\Omega) \to X^h$ and discrete Laplacian operator $\Delta_h : X \to X^h$ in the usual way by

$$(\Pi^h v - v, \chi) = 0, \quad (\Delta_h v, \chi) = -(\nabla v, \nabla \chi) \quad \forall \chi \in X^h. \tag{2.7}$$

With Δ_h, we can write $\bar{v}^h = (-\alpha^2 \Delta_h + \Pi^h)^{-1} v$ and $A_h = (-\alpha^2 \Delta_h + \Pi^h)$.

Remark 2.6. If Π^h is the L^2 projection on X^h and Π_1^h the projection on X^h with respect to to the H^1 semi-inner product (grad, grad) then $\Delta_h = \Pi^h \Delta_h = \Delta_h \Pi_1^h$. Further, Δ_h is extended from X^h to X by zero on the orthogonal complement of X^h with respect to (grad, grad).

Remark 2.7. For other (non-rotational) formulations of the nonlinearity, an attractive alternative is to define the differential filter by a discrete Stokes problem so as to preserve incompressibility approximately. In this case, given $\phi \in V$, $\bar{\phi}^h \in V^h$ would be defined by

$$\alpha^2(\nabla \bar{\phi}^h, \nabla \chi) + (\bar{\phi}^h, \chi) = (\phi, \chi) \quad \text{for all } \chi \in V^h.$$

Herein we study (2.6) which seems to be perfectly acceptable when working with the rotational form of the nonlinearity.

We begin by recalling from [5,42] some basic facts about discrete differential filters.

Lemma 2.8. *For $v \in X$, we have the following bounds for the discretely filtered and approximately deconvolved v*

$$\|\bar{v}^h\| \leqslant \|v\|, \quad \|\nabla \bar{v}^h\| \leqslant \|\nabla v\| \quad \text{and} \quad \|\nabla \times \bar{v}^h\| \leqslant \|\nabla v\|. \tag{2.8}$$

Proof. The proof of the first part of (2.8) follows from choosing $\chi = \bar{v}^h$ in (2.6), and applying Young's inequality. For the second inequality in (2.8), we note that the filter definition can be rewritten using Δ_h as

$$-\alpha^2(\Delta_h \bar{v}^h, \chi) + (\bar{v}^h, \chi) = (v, \chi) \quad \forall \chi \in X^h.$$

Choosing $\chi = \Delta_h \bar{v}^h$ and using the definition of Δ_h gives

$$\alpha^2 \|\Delta_h \bar{v}^h\|^2 + \|\nabla \bar{v}^h\|^2 = -(\nabla v, \nabla \bar{v}^h).$$

Young's inequality completes the proof. The last inequality follows from $\|\nabla \times \bar{v}^h\| \leqslant \|\nabla \bar{v}^h\|$ and the second inequality. □

Lemma 2.9. *For $\phi \in X$ and $\Delta\phi \in L^2(\Omega)$*

$$\alpha^2 ||\nabla(\phi - \bar{\phi}^h)||^2 + ||\phi - \bar{\phi}^h||^2 \leqslant C \inf_{v^h \in X^h} \{\alpha^2 ||\nabla(\phi - v^h)||^2 + ||\phi - v^h||^2\} + C\alpha^4 ||\Delta\phi||^2.$$

Proof. The functions ϕ and $\bar{\phi}^h$ satisfy, respectively for any $v^h \in X^h$

$$\alpha^2(\nabla \bar{\phi}^h, \nabla v^h) + (\bar{\phi}^h, v^h) = (\phi, v^h),$$
$$\alpha^2(\nabla \phi, \nabla v^h) + (\phi, v^h) = -\alpha^2(\Delta\phi, v^h) + (\phi, v^h).$$

If the error is denoted $e := \phi - \bar{\phi}^h$, subtraction gives for any $v^h \in X^h$

$$\alpha^2(\nabla e, \nabla v^h) + (e, v^h) = -\alpha^2(\Delta\phi, v^h).$$

The rest of the proof follows standard error analysis of finite element method. Let $\tilde{\phi} \in X^h$ be arbitrary and split the error as $e = (\phi - \tilde{\phi}) - (\bar{\phi}^h - \tilde{\phi})$. Rearranging the above error equation following that splitting, setting $v^h = \bar{\phi}^h - \tilde{\phi}$ and using the Cauchy–Schwarz–Young inequality and the triangle inequality completes the proof. □

To compress the analysis of both cases, it will be convenient to define two related trilinear forms that correspond to the regularized models.

Definition 2.10. (b_α and b_ω). Define b_α and $b_\omega : X \times X \times X \to \mathbb{R}$, as

$$b_\alpha(u, v, w) := ((\nabla \times u) \times \bar{v}^h, w), \quad \text{and}$$
$$b_\omega(u, v, w) := ((\nabla \times \bar{u}^h) \times v, w).$$

We shall assume that the solution to the NSE that is approximated by the model is a strong solution and in particular satisfies $u \in L^2(0,T;X) \cap L^\infty(0,T;L^2(\Omega)) \cap L^4(0,T;X)$, $p \in L^2(0,T;Q)$, $u_t \in L^2(0,T;X^*)$ and

$$(u_t, v) + (u \cdot \nabla u, v) - (p, \nabla \cdot v) + \nu(\nabla u, \nabla v) = (f, v) \quad \forall v \in X, \tag{2.9}$$
$$(q, \nabla \cdot u) = 0 \quad \forall q \in Q. \tag{2.10}$$

For notational clarity let $\nu(t_{n+1/2}) = \nu((t_n + t_{n+1})/2)$ for the continuous variable and $v_{n+1/2} = (v_n + v_{n+1})/2$ for both, continuous and discrete variables.

Algorithm 2.11. Full CN-FEM for NS-α or NS-$\bar{\omega}$

For $b = b_\alpha$ or b_ω.

Let $\Delta t > 0$, $(u_0, p_0) \in (X^h, Q^h)$, $f \in X^*$ and $T := M\Delta t$ for M an integer.

For $n = 0, 1, 2, \ldots, M-1$, find $(u_{n+1}^h, p_{n+1}^h) \in (X^h, Q^h)$ satisfying

$$\frac{1}{\Delta t}(u_{n+1}^h - u_n^h, v^h) + b(u_{n+1/2}^h, u_{n+1/2}^h, v^h) - (P_{n+1/2}^h, \nabla \cdot v^h) + \nu(\nabla u_{n+1/2}^h, \nabla v^h) = (f_{n+1/2}, v^h) \quad \forall v^h \in X^h, \tag{2.11}$$

and

$$\text{for the alpha model}: \ (\nabla \cdot \overline{u_{n+1}^h}^h, q^h) = 0 \quad \forall q^h \in Q^h, \tag{2.12}$$
$$\text{for the omega model}: \ (\nabla \cdot u_{n+1}^h, q^h) = 0 \quad \forall q^h \in Q^h. \tag{2.13}$$

Remark 1. Consider the NS-α model. Since the averaged term $\overline{u_{n+1}^h}^h$ in b_α is non-local, this must be implemented as a coupled system for $(u_{n+1}^h, w_{n+1}^h, p_{n+1}^h)$, where $w_{n+1}^h = \overline{u_{n+1}^h}^h$, of the following form

$$\frac{1}{\Delta t}(u_{n+1}^h - u_n^h, v^h) + b_\alpha\left(u_{n+1/2}^h, \frac{1}{2} w_{n+1}^h + \frac{1}{2}\overline{u_n^h}^h, v^h\right) - (P_{n+1/2}^h, \nabla \cdot v^h) + \nu(\nabla u_{n+1/2}^h, \nabla v^h) = (f_{n+1/2}, v^h) \quad \forall v^h \in X^h, \tag{2.14}$$

$$\alpha^2(\nabla w^h_{n+1}, \nabla\chi^h) + (w^h_{n+1}, \chi^h) = (u^h_{n+1}, \chi^h) \quad \forall \chi^h \in X^h, \tag{2.15}$$

$$(\nabla \cdot w^h_{n+1}, q^h) = 0 \quad \forall q^h \in Q^h. \tag{2.16}$$

Since (X^h, Q^h) satisfies the LBB^h condition, this is equivalent to

$$\frac{1}{\Delta t}(u^h_{n+1} - u^h_n, v^h) + b_\alpha(u^h_{n+1/2}, \frac{1}{2}w^h_{n+1} + \frac{1}{2}\overline{u^h_n}^h, v^h) + \nu(\nabla u^h_{n+1/2}, \nabla v^h) = (f_{n+1/2}, v^h) \quad \forall v^h \in X^h, \tag{2.17}$$

$$\alpha^2(\nabla w^h_{n+1}, \nabla\chi^h) + (w^h_{n+1}, \chi^h) = (u^h_{n+1}, \chi^h) \quad \forall \chi^h \in V^h. \tag{2.18}$$

At each time-step, the full CN method requires the solution of a large, coupled, nonlinear system whose 1–1 block's linearization is potentially highly non-symmetric and indefinite. To simplify the computations, we also consider an extrapolated version of the above, CNLE. Note that for the CNLE implementation of Algorithm 2.11, a choice must be made of which nonlinear term is to be extrapolated. Our choice is made based on the following two considerations:

- Unconditional energy stability, which implies the $\nabla \times u^h_{n+1}$ term must be the one to be extrapolated, and
- Efficiency, which implies the non-local, filtered term should be the one to be extrapolated.

These two constraints can both be satisfied when the $\nabla \times u$ term is filtered, which is the motivation for the precise form of the NS-$\bar{\omega}$ model and its treatment below.

Algorithm 2.12. Crank–Nicolson linear extrapolation scheme for NS-$\bar{\omega}$

Consider the NS-$\bar{\omega}$ model.
Define $E(\phi^h_n, \phi^h_{n-1}) = \frac{3}{2}\phi^h_n - \frac{1}{2}\phi^h_{n-1}$.
Let $\Delta t > 0$, $(u^h_0, P^h_0) \in (X^h, Q^h)$, $f \in X^*$ and $M := \frac{T}{\Delta t}$ and $(u^h_{-1}, P^h_{-1}) = (u^h_0, P^h_0)$.
For $n = 0, 1, 2, \cdots, M-1$, find $(u^h_{n+1}, P^h_{n+1}) \in (X^h, Q^h)$ satisfying

$$\frac{1}{\Delta t}(u^h_{n+1} - u^h_n, v^h) + b_\omega(E(u^h_n, u^h_{n-1}), u^h_{n+1/2}, v^h) - (P^h_{n+1/2}, \nabla \cdot v^h) + \nu(\nabla u^h_{n+1/2}, \nabla v^h) = (f_{n+1/2}, v^h) \quad \forall v^h \in X^h, \tag{2.19}$$

$$(\nabla \cdot u^h_{n+1}, q^h) = 0 \quad \forall q^h \in Q^h. \tag{2.20}$$

Note that the non-local, filtered term, $\nabla \times \overline{E(u^h_n, u^h_{n-1})}^h$, is an explicit and inexpensive computation on a known function. Each step of the above requires the solution of one linear (rather than nonlinear for CN) (Oseen like) system in which the 1–1 block has positive definite symmetric part (rather than possibly both non-symmetric and indefinite for CN). For CNLE for the NS-$\bar{\omega}$ model, backward Euler suffices for the first time-step. For $n = 0$, this is equivalent to (u_{-1}, P_{-1}) constant extrapolation.

Remark 2.13. It is also interesting to consider an analogous algorithm with quadratic extrapolation which has better stability and accuracy properties. It can be implemented just as Algorithm 2.12 by replacing the linear extrapolation $E(\phi^h_n, \phi^h_{n-1}) = \frac{3}{2}\phi^h_n - \frac{1}{2}\phi^h_{n-1}$ with $E(\phi^h_n, \phi^h_{n-1}, \phi^h_{n-2}) = \frac{15}{8}\phi^h_n - \frac{10}{8}\phi^h_{n-1} + \frac{3}{8}\phi^h_{n-2}$. The error in quadratic extrapolation is higher order than that of the base CN and thus might be preferable for problems involving delicate solution behavior.

Another possible advantage of NS-$\bar{\omega}$ is that it is a rotational form model. Rotational form solvers preconditioners have been studied extensively for the Navier–Stokes equations [39,45], and thus the ability for NS-$\bar{\omega}$ to be implemented for efficient large scale computations could be a feasible extension of such work.

CNLE for the Navier–Stokes equations was first investigated in [1] by Baker. It is second order in time, unconditionally stable and linearly implicit. The convergence analysis of CNLE follows closely but it is technically longer than the full CN method that we perform in Section 3.

Lemma 2.14. *Assume $u \in C^0(t_n, t_{n+1}; L^2(\Omega))$. If u is twice differentiable in time and $u_{tt} \in L^2((t_n, t_{n+1}) \times \Omega)$ then*

$$\|u_{n+1/2} - u(t_{n+1/2})\|^2 \leqslant \frac{1}{48}(\Delta t)^3 \int_{t_n}^{t_{n+1}} \|u_{tt}\|^2 dt. \tag{2.21}$$

If $u_{ttt} \in L^2((t_n, t_{n+1}) \times \Omega)$ then

$$\left\|\frac{u_{n+1} - u_n}{\Delta t} - u_t(t_{n+1/2})\right\|^2 \leqslant \frac{1}{1280}(\Delta t)^3 \int_{t_n}^{t_{n+1}} \|u_{ttt}\|^2 dt \quad \text{and} \tag{2.22}$$

if $\nabla u \in C^0(t_n, t_{n+1}; L^2(\Omega))$ and $\nabla u_{tt} \in L^2((t_n, t_{n+1}) \times \Omega)$ then

$$\|\nabla(u_{n+1/2} - u(t_{n+1/2}))\|^2 \leqslant \frac{(\Delta t)^3}{48} \int_{t_n}^{t_{n+1}} \|\nabla u_{tt}\|^2 dt. \tag{2.23}$$

The proof of Lemma 2.14 is based on the Taylor expansion with remainder. It is more of technical nature and therefore omitted herein. The error analysis uses a discrete Gronwall inequality, recalled from [27], for example.

Lemma 2.15. Discrete Gronwall Lemma *Let Δt, H, and a_n, b_n, c_n, d_n (for integers $n \geqslant 0$) be nonnegative numbers such that*

$$a_l + \Delta t \sum_{n=0}^{l} b_n \leqslant \Delta t \sum_{n=0}^{l} d_n a_n + \Delta t \sum_{n=0}^{l} c_n + H \quad \text{for } l \geqslant 0. \tag{2.24}$$

Suppose that $d_n \Delta t < 1$ $\forall n$. Then,

$$a_l + \Delta t \sum_{n=0}^{l} b_n \leqslant \exp\left(\Delta t \sum_{n=0}^{l} \frac{d_n}{1 - \Delta t d_n}\right)\left(\Delta t \sum_{n=0}^{l} c_n + H\right) \quad \text{for } l \geqslant 0. \tag{2.25}$$

3. Analysis of full Crank–Nicolson scheme for the NS-$\bar{\omega}$ model

In this section, we show that solutions of the CN schemes for both regularizations are unconditionally stable and well defined. We prove that the CN–FEM is optimally convergent to solutions of the NSE. (The case of the NS-α model is considerably more delicate, see Connors [11].) This error analysis, already technical, can be extended to the CNLE (or CNQE) time stepping method, and grad–div stabilization.

Lemma 3.1. *Consider the NS-$\bar{\omega}$ model and the schemes in Algorithms 2.11 and 2.12 (CN and CNLE, respectively). A solution u^l_h, $l = 1, \ldots M$, exists at each time-step. Both schemes are unconditionally stable: their solutions satisfy the following á priori bound:*

$$\|u^h_M\|^2 + \nu\Delta t \sum_{n=0}^{M-1} \|\nabla u^h_{n+1/2}\|^2 \leqslant \|u^h_0\|^2 + \frac{\Delta t}{\nu} \sum_{n=0}^{M-1} \|f_{n+1/2}\|^2_*. \tag{3.1}$$

Proof. The existence of a solution u^n_h to the schemes in Algorithms 2.11 and 2.12 follows from the Leray–Schauder Principle [55]. The main step is deriving an á priori estimate, which can be obtained by setting $v^h = u^h_{n+1/2}$ both in (2.11) and (2.19). The nonlinear term in the two schemes considered vanishes with this choice. Thus,

$$\frac{1}{2\Delta t}(\|u^h_{n+1}\|^2 - \|u^h_n\|^2) + \nu\|\nabla u^h_{n+1/2}\|^2 \leqslant \frac{1}{2\nu}\|f_{n+1/2}\|^2_* + \frac{\nu}{2}\|\nabla u^h_{n+1/2}\|^2 \quad \text{for every } n,$$

i.e.,

$$\frac{1}{\Delta t}(\|u^h_{n+1}\|^2 - \|u^h_n\|^2) + \nu\|\nabla u^h_{n+1/2}\|^2 \leqslant \frac{1}{\nu}\|f_{n+1/2}\|^2_*, \quad \text{for every } n.$$

Summing from $n = 0 \ldots M-1$ gives the desired result. □

Remark 3.2. Since the kinetic energy and energy dissipation of NS-$\bar{\omega}$, KE_ω and ε_ω, take the usual form, Lemma 3.1 implies

$$KE_\omega(u^h_M) + \nu\frac{\Delta t}{2}\sum_{n=0}^{M-1}\varepsilon_\omega(u^h_{n+1/2}) \leqslant KE_\omega(u^h_0) + \frac{\Delta t}{2\nu}\sum_{n=0}^{M-1}\|f_{n+1/2}\|^2_*. \quad (3.2)$$

Thus if $\nu = f = 0$, $KE_\omega(u^h_M) = KE_\omega(u^h_0)$. Hence Algorithms 2.11 and 2.12 are energy conserving.

Next we review stability of the CN method for NS-α. For NS-α it is stable with respect to a modified kinetic energy with a modified energy dissipation, given by

$$KE_\alpha(u) := \frac{1}{2}\|\bar{u}^h\|^2 + \frac{\alpha^2}{2}\|\nabla\bar{u}^h\|^2, \quad \varepsilon_\alpha(u) := \nu||\nabla\bar{u}^h||^2 + \nu\alpha^2||\Delta^h\bar{u}^h||^2.$$

Discrete versions of these two are also exactly conserved by the fully discrete schemes. We begin by considering the case of NS-α.

Lemma 3.3. *Consider Algorithm 2.11. The scheme (2.11, 2.12) is well defined and unconditionally stable. A solution u^l_h, $l = 1, \ldots, M$, exists at each time-step that satisfies the following á priori bound:*

$$KE_\alpha(u^h_M) + \frac{\Delta t}{2}\sum_{n=0}^{M-1}\varepsilon_\alpha(u^h_{n+1/2}) \leqslant KE_\alpha(u^h_0) + \frac{\Delta t}{2\nu}\sum_{n=0}^{M-1}\|f_{n+1/2}\|^2_*. \quad (3.3)$$

If $\nu = f = 0$ then,

$$KE_\alpha(u^h_M) = KE_\alpha(u^h_0). \quad (3.4)$$

Proof. The key for existence and stability is the á priori estimate and the key for the á priori estimate is the exact choice of test function which makes the nonlinear term vanish. Thus we first note that choosing $v^h = \overline{u^h_{n+1/2}}^h$ does this since

$$b^*_\alpha(u^h_{n+1/2}, u^h_{n+1/2}, \overline{u^h_{n+1/2}}^h) = 0.$$

With this choice, and $q^h = P^h_{n+1/2}$, we have for NS-alpha:

$$\frac{1}{\Delta t}(u^h_{n+1} - u^h_n, \overline{u^h_{n+1/2}}^h) - (P^h_{n+1/2}, \nabla\cdot\overline{u^h_{n+1/2}}^h) + \nu(\nabla u^h_{n+1/2}, \nabla\overline{u^h_{n+1/2}}^h) = (f_{n+1/2}, \overline{u^h_{n+1/2}}^h),$$

$$(\nabla\cdot\overline{u^h_{n+1/2}}^h, P^h_{n+1/2}) = 0.$$

Adding the equations the Bernoulli pressure term drops out as well. We thus obtain

$$\frac{1}{\Delta t}(u^h_{n+1} - u^h_n, \overline{u^h_{n+1/2}}^h) + \nu(\nabla u^h_{n+1/2}, \nabla\overline{u^h_{n+1/2}}^h) = (f_{n+1/2}, \overline{u^h_{n+1/2}}^h).$$

Consider the viscous term. This can be written as (using the fact that the operators involved commute on X^h)

$$\begin{aligned}\nu(\nabla u^h_{n+1/2}, \nabla\overline{u^h_{n+1/2}}^h) &= -\nu(\Delta^h u^h_{n+1/2}, \overline{u^h_{n+1/2}}^h)\\ &= -\nu(\Delta^h A_h\overline{u^h_{n+1/2}}^h, \overline{u^h_{n+1/2}}^h)\\ &= \nu(\nabla\overline{u^h_{n+1/2}}^h, \nabla\overline{u^h_{n+1/2}}^h)\\ &\quad + \nu\alpha^2(\Delta^h\overline{u^h_{n+1/2}}^h, \Delta^h\overline{u^h_{n+1/2}}^h)\\ &= \nu||\nabla\overline{u^h_{n+1/2}}^h||^2 + \nu\alpha^2||\Delta^h\overline{u^h_{n+1/2}}^h||^2\\ &= \varepsilon_\alpha(u^h_{n+1/2}).\end{aligned}$$

Similarly, the time difference term can be rewritten as

$$\begin{aligned}\frac{1}{\Delta t}(u^h_{n+1} - u^h_n, \overline{u^h_{n+1/2}}^h) &= \frac{1}{\Delta t}(A_h\overline{u^h_{n+1}}^h - A_h\overline{u^h_n}^h, \overline{u^h_{n+1/2}}^h)\\ &= \frac{1}{\Delta t}(\overline{u^h_{n+1}}^h - \overline{u^h_n}^h, \overline{u^h_{n+1/2}}^h)\\ &\quad + \frac{\alpha^2}{\Delta t}(\nabla\overline{u^h_{n+1}}^h - \nabla\overline{u^h_n}^h, \nabla\overline{u^h_{n+1/2}}^h)\\ &= \frac{1}{2\Delta t}(\|\overline{u^h_{n+1}}^h\|^2 - \|\overline{u^h_n}^h\|^2) + \frac{\alpha^2}{2\Delta t}(\|\nabla\overline{u^h_{n+1}}^h\|^2\\ &\quad - \|\nabla\overline{u^h_{n+1}}^h\|^2) = \frac{1}{\Delta t}(KE_\alpha(u^h_{n+1}) - KE_\alpha(u^h_n)).\end{aligned}$$

Thus,

$$\frac{1}{\Delta t}(KE_\alpha(u^h_{n+1}) - KE_\alpha(u^h_n)) + \varepsilon_\alpha(u^h_{n+1/2}) \leqslant \frac{1}{2\nu}\|f_{n+1/2}\|^2_* + \frac{\nu}{2}\|\nabla\overline{u^h_{n+1/2}}^h\|^2, \quad \text{for every } n,$$

i.e.,

$$\frac{1}{\Delta t}(KE_\alpha(u^h_{n+1}) - KE_\alpha(u^h_n)) + \frac{1}{2}\varepsilon_\alpha(u^h_{n+1/2}) \leqslant \frac{1}{2\nu}\|f_{n+1/2}\|^2_*.$$

Summing from $n = 0 \ldots M-1$ gives the desired result. The á priori bound and an argument using the Leray–Schauder fixed point theorem yields existence of the approximate solution at each time level as well. □

Our main convergence result for the discrete NS-$\bar{\omega}$ model is given next.

Theorem 3.4. Convergence for discrete NS-omega regularization *Consider the discrete NS-$\bar{\omega}$ model. Let $(u(t), P(t))$ be a smooth, strong solution of the NSE satisfying either no-slip or periodic with zero-mean boundary conditions such that the norms of $(u(t), P(t))$ on the right hand side of (3.5) and (3.6) are finite. Suppose (u^h_0, P^h_0) are the V_h and Q_h interpolants of $(u(0), P(0))$, respectively. Suppose (u^h, P^h) is the CN approximation (2.11)–(2.13) of the NS-$\bar{\omega}$ model. Then for Δt small enough there is a constant $C = C(u, P)$ such that*

$$|||u - u^h|||_{\infty,0} \leqslant F(\Delta t, h, \alpha) + Ch^{k+1}|||u|||_{\infty,k+1}, \quad (3.5)$$

$$\left(\nu\Delta t\sum_{n=0}^{M-1}\|\nabla(u_{n+1/2} - (u^h_{n+1} + u^h_n)/2)\|^2\right)^{1/2} \leqslant F(\Delta t, h, \alpha) + C\nu^{1/2}(\Delta t)^2\|\nabla u_{tt}\|_{2,0} + C\nu^{1/2}h^k|||u|||_{2,k+1}, \quad (3.6)$$

where

$$\begin{aligned}F(\Delta t, h, \alpha) := C^*\Big\{&\nu^{-1/2}h^{k+1/2}\Big(|||u|||^2_{4,k+1} + |||\nabla u|||^2_{4,0}\Big) + \nu^{1/2}h^k|||u|||_{2,k+1}\\ &+ \nu^{-1/2}h^k\Big(|||u|||^2_{4,k+1} + \nu^{-1/2}(\|u^h_0\| + \nu^{-1/2}\|f\|_{2,*})\Big)\\ &+ \nu^{-1/2}h^{s+1}|||P_{1/2}|||_{2,s+1} + \nu^{-1/2}\alpha^2|||u|||_{4,1}|||u|||_{4,3}\\ &+ (\Delta t)^2\Big(\|u_{ttt}\|_{2,0} + \nu^{-1/2}\|P_{tt}\|_{2,0} + \|f_{tt}\|_{2,0} + \nu^{1/2}\|\nabla u_{tt}\|_{2,0}\\ &+ \nu^{-1/2}\|\nabla u_{tt}\|^2_{4,0} + \nu^{-1/2}|||\nabla u|||^2_{4,0} + \nu^{-1/2}|||\nabla u_{1/2}|||^2_{4,0}\Big)\Big\}.\end{aligned} \quad (3.7)$$

Remark 3.5. The constant C^* arising from Gronwall's lemma depends on ν like $exp(\nu^{-3}T)$ and the smallness assumption on the time-step is $\Delta t < C(\nu^{-3}|||\nabla u|||^4_{\infty,0} + 1)^{-1}$. We believe that this last condition on Δt is improvable.

Corollary 3.6. *Suppose that in addition to the assumptions made in Theorem 3.4, the finite element spaces X^h and Q^h are composed of Taylor–Hood elements. Suppose u is smooth in the sense that the indicated norms on the right hand side of (3.5) and (3.6) are finite for $k = 2$ and $s = 1$. Then the error in the CN scheme for the model (2.11)–(2.13), is of the order*

$$|||u-u^h|||_{\infty,0}+\left(\nu\Delta t\sum_{n=1}^{M}\|\nabla(u_{n+1/2}-u^h_{n+1/2})\|^2\right)^{1/2}$$
$$=O(h^2+\Delta t^2+\alpha^2). \tag{3.8}$$

Proof of Theorem 3.4. Note that for $u,v,w,\in X$, by adding and subtracting terms, we can write

$$b_\omega(u,v,w)=((\nabla\times u)\times v,w)-\text{filtering error},$$

specifically

$$b_\omega(u,v,w)=((\nabla\times u)\times v,w)\ -((\nabla\times u-\nabla\times\bar{u}^h)\times v,w).$$

Define the filtering error accordingly:

$$FE=FE_\omega(u,v,w):=((\nabla\times u-\nabla\times\bar{u}^h)\times v,w).$$

At time $t_{n+1/2}$, the solution of the NSE (u,P) satisfies

$$\left(\frac{u_{n+1}-u_n}{\Delta t},v^h\right)+b_\omega(u_{n+1/2},u_{n+1/2},v^h)+\nu(\nabla u_{n+1/2},\nabla v^h)$$
$$-(P_{n+1/2},\nabla\cdot v^h)=(f_{n+1/2},v^h)+Intp(u^n,P^n;v^h), \tag{3.9}$$

for all $v^h\in V^h$. The term $Intp(u_n,P_n;v^h)$ collects the interpolation error, the above filtering error and the consistency error. It is given by

$$Intp(u_n,p_n;v^h)$$
$$=\left(\frac{u_{n+1}-u_n}{\Delta t}-u_t(t_{n+1/2}),v^h\right)+\nu(\nabla u_{n+1/2}-\nabla u(t_{n+1/2}),\nabla v^h)$$
$$+b_\omega(u_{n+1/2},u_{n+1/2},v^h)-b_\omega(u(t_{n+1/2}),u(t_{n+1/2}),v^h)$$
$$-FE(u_{n+1/2},u_{n+1/2},v^h)-(P_{n+1/2}-P(t_{n+1/2}),\nabla\cdot v^h)$$
$$+(f(t_{n+1/2})-f_{n+1/2},v^h). \tag{3.10}$$

Subtracting (3.9) from (2.11) and letting $e_n=u_n-u^h_n$ we have

$$\frac{1}{\Delta t}(e_{n+1}-e_n,v^h)+b_\omega(u_{n+1/2},u_{n+1/2},v^h)$$
$$-b_\omega(u^h_{n+1/2},u^h_{n+1/2},v^h)+\nu(\nabla e_{n+1/2},\nabla v^h)$$
$$=(P_{n+1/2},\nabla\cdot v^h)+Intp(u_n,p_n;v^h)\quad\forall v^h\in V^h. \tag{3.11}$$

Decompose the error as $e_n=(u_n-U_n)-(u^h_n-U_n):=\eta_n-\phi^h_n$ where $\phi^h_n\in V^h$, and U is the L^2 projection of u in V^h. Setting $v^h=\phi^h_{n+1/2}$ in (3.11) and using $(q,\nabla\cdot\phi_{n+1/2})=0$ for all $q\in Q^h$ we obtain

$$(\phi^h_{n+1}-\phi^h_n,\phi^h_{n+1/2})+\nu\Delta t\|\nabla\phi^h_{n+1/2}\|$$
$$+\Delta tb_\omega(u^h_{n+1/2},e_{n+1/2},\phi^h_{n+1/2})$$
$$+\Delta tb_\omega(e_{n+1/2},u_{n+1/2},\phi^h_{n+1/2})$$
$$=(\eta_{n+1}-\eta_n,\phi^h_{n+1/2})+\Delta t\nu(\nabla\eta_{n+1/2},\nabla\phi^h_{n+1/2})$$
$$+\Delta t(P_{n+1/2}-q,\nabla\cdot\phi^h_{n+1/2})+\Delta tIntp(u_n,p_n;v^h), \tag{3.12}$$

i.e.

$$\frac{1}{2}(\|\phi^h_{n+1}\|-\|\phi^h_n\|)+\nu\Delta t\|\nabla\phi^h_{n+1/2}\|$$
$$=(\eta_{n+1}-\eta_n,\phi^h_{n+1/2})+\Delta t\nu(\nabla\eta_{n+1/2},\nabla\phi^h_{n+1/2})$$
$$-\Delta tb_\omega(\eta_{n+1/2},u_{n+1/2},\phi^h_{n+1/2})$$
$$+\Delta tb_\omega(\phi^h_{n+1/2},u_{n+1/2},\phi^h_{n+1/2})$$
$$-\Delta tb_\omega(u^h_{n+1/2},\eta_{n+1/2},\phi^h_{n+1/2})+\Delta t(P_{n+1/2}-q,\nabla\cdot\phi^h_{n+1/2})$$
$$+\Delta tIntp(u_n,p_n;\phi^h_{n+1/2}). \tag{3.13}$$

We now bound the terms in the RHS of (3.13) individually. According to the choice of U, $(\eta_{n+1}-\eta_n,\phi^h_{n+1/2})=0$. The Cauchy–Schwarz and Young's inequalities give

$$\nu\Delta t(\nabla\eta_{n+1/2},\nabla\phi^h_{n+1/2})\leqslant\nu\Delta t\|\nabla\eta_{n+1/2}\|\|\nabla\phi^h_{n+1/2}\|$$
$$\leqslant\frac{\nu\Delta t}{12}\|\nabla\phi^h_{n+1/2}\|^2+C\nu\Delta t\|\nabla\eta_{n+1/2}\|^2, \tag{3.14}$$

$$\Delta t(P_{n+1/2}-q,\nabla\cdot\phi^h_{n+1/2})\leqslant C\Delta t\|P_{n+1/2}-q\|\|\nabla\phi^h_{n+1/2}\|$$
$$\leqslant\frac{\nu\Delta t}{12}\|\nabla\phi^h_{n+1/2}\|^2+C\Delta t\nu^{-1}\|P_{n+1/2}-q\|^2. \tag{3.15}$$

Lemmas 2.2 and 2.8 and standard inequalities give

$$\Delta tb_\omega(\eta_{n+1/2},u_{n+1/2},\phi^h_{n+1/2})\leqslant C\Delta t\|\nabla\overline{\eta_{n+1/2}}^h\|\|\nabla u_{n+1/2}\|\|\nabla\phi^h_{n+1/2}\|$$
$$\leqslant C\Delta t\|\nabla\eta_{n+1/2}\|\|\nabla u_{n+1/2}\|\|\nabla\phi^h_{n+1/2}\|$$
$$\leqslant\frac{\nu\Delta t}{12}\|\nabla\phi^h_{n+1/2}\|^2$$
$$+C\Delta t\nu^{-1}\|\nabla\eta_{n+1/2}\|^2\|\nabla u_{n+1/2}\|^2. \tag{3.16}$$

$$\Delta tb_\omega(\phi^h_{n+1/2},u_{n+1/2},\phi^h_{n+1/2})$$
$$=\Delta t((\nabla\times\overline{\phi^h_{n+1/2}}^h)\times u_{n+1/2},\phi^h_{n+1/2})$$
$$\leqslant C\Delta t\|\nabla\times\overline{\phi^h_{n+1/2}}^h\|\|\nabla u_{n+1/2}\|\|\phi^h_{n+1/2}\|^{1/2}\|\nabla\phi^h_{n+1/2}\|^{1/2}$$
$$\leqslant C\Delta t\|\phi^h_{n+1/2}\|^{1/2}\|\nabla\phi^h_{n+1/2}\|^{3/2}\|\nabla u_{n+1/2}\|$$
$$\leqslant\frac{\nu\Delta t}{24}\|\nabla\phi^h_{n+1/2}\|^2+C\Delta t\nu^{-3}\|\phi^h_{n+1/2}\|^2\|\nabla u_{n+1/2}\|^4. \tag{3.17}$$

The final trilinear term requires a bit more effort. Begin by splitting the first entry of this term by adding and subtracting $u_{n+1/2}$, followed by rewriting the resulting error term as pieces inside and out of the finite element space.

$$\Delta tb_\omega(u^h_{n+1/2},\eta_{n+1/2},\phi^h_{n+1/2})=\Delta tb_\omega(\eta_{n+1/2},\eta_{n+1/2},\phi^h_{n+1/2})$$
$$+\Delta tb_\omega(\phi^h_{n+1/2},\eta_{n+1/2},\phi^h_{n+1/2})$$
$$+\Delta tb_\omega(u_{n+1/2},\eta_{n+1/2},\phi^h_{n+1/2}). \tag{3.18}$$

We bound each of the terms on the right hand side of (3.18) using the same inequalities and lemmas as above:

$$\Delta tb_\omega(\eta_{n+1/2},\eta_{n+1/2},\phi^h_{n+1/2})$$
$$\leqslant\Delta t\|\nabla\times\overline{\eta_{n+1/2}}^h\|\|\nabla\eta_{n+1/2}\|\|\nabla\phi^h_{n=1/2}\|$$
$$\leqslant\Delta t\|\nabla\eta_{n+1/2}\|^2\|\nabla\phi^h_{n+1/2}\|$$
$$\leqslant\frac{\nu\Delta t}{24}\|\nabla\phi^h_{n+1/2}\|^2+C\Delta t\nu^{-1}\|\nabla\eta_{n+1/2}\|^4, \tag{3.19}$$

$$\Delta tb_\omega(\phi^h_{n+1/2},\eta_{n+1/2},\phi^h_{n+1/2})$$
$$\leqslant C\Delta t\|\nabla\phi^h_{n+1/2}\|^{3/2}\|\nabla\eta_{n+1/2}\|\|\phi^h_{n+1/2}\|$$
$$\leqslant\frac{\nu\Delta t}{24}\|\nabla\phi^h_{n+1/2}\|^2+C\Delta t\nu^{-3}\|\nabla\eta_{n+1/2}\|^4\|\phi^h_{n+1/2}\|^2, \tag{3.20}$$

$$\Delta tb_\omega(u_{n+1/2},\eta_{n+1/2},\phi^h_{n+1/2})\leqslant\Delta t\|\nabla\times\overline{u_{n+1/2}}^h\|\|\nabla\eta_{n+1/2}\|\|\nabla\phi^h_{n+1/2}\|$$
$$\leqslant\frac{\nu\Delta t}{24}\|\nabla\phi^h_{n+1/2}\|^2$$
$$+C\Delta t\nu^{-1}\|\nabla\eta_{n+1/2}\|^2\|\nabla u_{n+1/2}\|^2. \tag{3.21}$$

Combining (3.14)–(3.21) and summing from $n=0$ to $M-1$ (assuming that $\|\phi_0^h\|=0$) reduces (3.13) to

$$\begin{aligned}
&\|\phi_M^h\|^2+\nu\Delta t\sum_{n=0}^{M-1}\|\nabla\phi_{n+1/2}^h\|^2\\
&\leqslant C\Delta t\Bigg\{\sum_{n=0}^{M-1}C\nu^{-3}(\|\nabla u_{n+1/2}\|^4\\
&+\|\nabla\eta_{n+1/2}\|^4)\|\phi_{n+1/2}^h\|^2 \qquad (3.22)\\
&+\sum_{n=0}^{M-1}\left((\nu+\nu^{-1})\|\nabla\eta_{n+1/2}\|^2+\nu^{-1}\|\nabla\eta_{n+1/2}\|^4\right)\\
&+\sum_{n=0}^{M-1}\nu^{-1}\|\eta_{n+1/2}\|\|\nabla\eta_{n+1/2}\|\|\nabla u_{n+1/2}\|^2\\
&+\sum_{n=0}^{M-1}\|\nabla\times\overline{u_{n+1/2}^h}^h\|\|\nabla\eta_{n+1/2}\|\|\phi_{n+1/2}^h\|^{\frac12}\|\nabla\phi_{n+1/2}^h\|^{\frac12}\\
&+\sum_{n=0}^{M-1}\nu^{-1}\|P_{n+1/2}-q\|^2\\
&+\sum_{n=0}^{M-1}|Intp(u_n,p_n;\phi_{n+1/2}^h)|\Bigg\}. \qquad (3.23)
\end{aligned}$$

Now, we continue to bound the terms on the RHS of (3.23). We have that

$$\begin{aligned}
\Delta t\sum_{n=0}^{M-1}C\nu\|\nabla\eta_{n+1/2}\|^2&\leqslant\Delta tC(\nu+\nu^{-1})\sum_{n=0}^{M}\|\nabla\eta_n\|^2\\
&\leqslant\Delta tC(\nu+\nu^{-1})\sum_{n=0}^{M}h^{2k}|u^n|_{k+1}^2\\
&\leqslant C(\nu+\nu^{-1})h^{2k}\|u\|_{2,k+1}^2, \qquad (3.24)
\end{aligned}$$

and similarly,

$$\begin{aligned}
\Delta t\sum_{n=0}^{M-1}C\nu^{-1}\|\nabla\eta_{n+1/2}\|^4&\leqslant\Delta tC\nu^{-1}\sum_{n=0}^{M}\|\nabla\eta_n\|^4\\
&\leqslant\Delta tC\nu^{-1}\sum_{n=0}^{M}h^{4k}|u^n|_{k+1}^4\\
&\leqslant C\nu^{-1}h^{4k}\|u\|_{2,k+1}^4. \qquad (3.25)
\end{aligned}$$

For the term

$$\begin{aligned}
&\Delta t\sum_{n=0}^{M-1}C\nu^{-1}\|\nabla\eta_{n+1/2}\|^2\|\nabla u_{n+1/2}\|^2\\
&\leqslant C\nu^{-1}\Delta th^{2k}\sum_{n=0}^{M-1}(|u_{n+1}|_{k+1}^2+|u_n|_{k+1}^2)\|\nabla u_{n+1/2}\|^2\\
&\leqslant C\nu^{-1}\Delta th^{2k}\left(\|u\|_{4,k+1}^4+\|\nabla u\|_{4,0}^4\right). \qquad (3.26)
\end{aligned}$$

From (2.14),

$$\begin{aligned}
&\Delta t\sum_{n=0}^{M-1}C\nu^{-1}\|P_{n+1/2}-q\|^2\\
&\leqslant C\nu^{-1}\Delta t\sum_{n=0}^{M-1}\|P(t_{n+1/2})-q\|^2+\|P_{n+1/2}-P(t_{n+1/2})\|^2\\
&\leqslant C\nu^{-1}\left(h^{2s+2}\Delta t\sum_{n=0}^{M-1}\|P(t_{n+1/2})\|_{s+1}^2+\Delta t\sum_{n=0}^{M-1}\frac{1}{48}(\Delta t)^3\int_{t_n}^{t_{n+1}}\|p_{tt}\|^2dt\right)\\
&\leqslant C\nu^{-1}\left(h^{2s+2}\|p_{1/2}\|_{2,s+1}^2+(\Delta t)^4\|p_{tt}\|_{2,0}^2\right). \qquad (3.27)
\end{aligned}$$

We now bound the terms in $Intp(u_n,p_n;\phi_{n+1/2}^h)$. Using Cauchy–Schwarz and Young's inequalities, Taylor's theorem, and Lemmas 2.8 and 2.9,

$$\begin{aligned}
&\left(\frac{u^{n+1}-u_n}{\Delta t}-u_t(t_{n+1/2}),\phi_{n+1/2}^h\right)\\
&\leqslant\frac12\|\phi_{n+1/2}^h\|^2+\frac12\|\frac{u^{n+1}-u_n}{\Delta t}-u_t(t_{n+1/2})\|^2\\
&\leqslant\frac12\|\phi_{n+1}^h\|^2+\frac12\|\phi_n^h\|^2+\frac12\frac{(\Delta t)^3}{1280}\int_{t_n}^{t_{n+1}}\|u_{ttt}\|^2dt, \qquad (3.28)
\end{aligned}$$

$$\begin{aligned}
&(P_{n+1/2}-P(t_{n+1/2}),\nabla\cdot\phi_{n+1/2}^h)\\
&\leqslant\varepsilon_1\nu\|\nabla\phi_{n+1/2}^h\|^2+C\nu^{-1}\|P_{n+1/2}-P(t_{n+1/2})\|^2\\
&\leqslant\varepsilon_1\nu\|\nabla\phi_{n+1/2}^h\|^2+C\nu^{-1}\frac{(\Delta t)^3}{48}\int_{t_n}^{t_{n+1}}\|p_{tt}\|^2dt, \qquad (3.29)
\end{aligned}$$

$$\begin{aligned}
&(f(t_{n+1/2})-f_{n+1/2},\phi_{n+1/2}^h)\\
&\leqslant\frac12\|\phi_{n+1/2}^h\|^2+\frac12\|f(t_{n+1/2})-f_{n+1/2}\|^2\\
&\leqslant\frac12\|\phi_{n+1}^h\|^2+\frac12\|\phi_n^h\|^2+\frac{(\Delta t)^3}{48}\int_{t_n}^{t_{n+1}}\|f_{tt}\|^2dt, \qquad (3.30)
\end{aligned}$$

$$\begin{aligned}
&\nu(\nabla u_{n+1/2}-\nabla u(t_{n+1/2}),\nabla\phi_{n+1/2}^h)\\
&\leqslant\varepsilon_2\nu\|\nabla\phi_{n+1/2}^h\|^2+C\nu\|\nabla u_{n+1/2}-\nabla u(t_{n+1/2})\|^2\\
&\leqslant\varepsilon_2\nu\|\nabla\phi_{n+1/2}^h\|^2+C\nu\frac{(\Delta t)^3}{48}\int_{t_n}^{t_{n+1/2}}\|\nabla u_{tt}\|^2dt, \qquad (3.31)
\end{aligned}$$

$$\begin{aligned}
&b_\omega(u_{n+1/2},u_{n+1/2},\phi_{n+1/2}^h)-b_\omega(u(t_{n+1/2}),u(t_{n+1/2}),\phi_{n+1/2}^h)\\
&=b_\omega(u_{n+1/2}-u(t_{n+1/2}),u_{n+1/2},\phi_{n+1/2}^h)+b_\omega(u(t_{n+1/2}),u_{n+1/2}\\
&\quad-u(t_{n+1/2}),\phi_{n+1/2}^h)\\
&\leqslant C\|\nabla\times\overline{(u_{n+1/2}-u(t_{n+1/2}))}^h\|\|\nabla\phi_{n+1/2}^h\|\left(\|\nabla u_{n+1/2}\|+\|\nabla u(t_{n+1/2})\|\right)\\
&\leqslant C\|\nabla(u_{n+1/2}-u(t_{n+1/2}))\|\|\nabla\phi_{n+1/2}^h\|\left(\|\nabla u_{n+1/2}\|+\|\nabla u(t_{n+1/2})\|\right)\\
&\leqslant C\nu^{-1}\left(\|\nabla u_{n+1/2}\|^2+\|\nabla u(t_{n+1/2})\|^2\right)\frac{(\Delta t)^3}{48}\int_{t_n}^{t_{n+1}}\|\nabla u_{tt}\|^2dt\\
&\quad+\varepsilon_3\nu\|\nabla\phi_{n+1/2}^h\|^2\\
&\leqslant C\nu^{-1}\frac{(\Delta t)^3}{48}\left(\int_{t_n}^{t_{n+1}}2(\|\nabla u_{n+1/2}\|^4+\|\nabla u(t_{n+1/2})\|^4)dt\right.\\
&\quad\left.+\int_{t_n}^{t_{n+1}}\|\nabla u_{tt}\|^4dt\right)+\varepsilon_3\nu\|\nabla\phi_{n+1/2}^h\|^2\\
&\leqslant C\nu^{-1}(\Delta t)^4(\|\nabla u_{n+1/2}\|^4+\|\nabla u(t_{n+1/2})\|^4)\\
&\quad+C\nu^{-1}(\Delta t)^3\int_{t_n}^{t_{n+1}}\|\nabla u_{tt}\|^4dt+\varepsilon_3\nu\|\nabla\phi_{n+1/2}^h\|^2. \qquad (3.32)
\end{aligned}$$

Next we will bound the filtering error using the definition of the discrete filter.

$$\begin{aligned}
FE&\leqslant\left|(\nabla\times u_{n+1/2}-\nabla\times\overline{u_{n+1/2}}^h\times u_{n+1/2},\phi_{n+1/2}^h)\right|\\
&\leqslant C\|\nabla\times(u_{n+1/2}-\overline{u_{n+1/2}}^h)\|\|\nabla u_{n+1/2}\|\|\nabla\phi_{n+1/2}^h\|\\
&\leqslant\varepsilon_4\nu\|\nabla\phi_{n+1/2}^h\|^2+C\nu^{-1}\alpha^4\|\nabla u_{n+1/2}\|^2\|\nabla\Delta^h\overline{u_{n+1/2}}^h\|^2\\
&\leqslant\varepsilon_4\nu\|\nabla\phi_{n+1/2}^h\|^2+C\nu^{-1}\alpha^4\|\nabla u_{n+1/2}\|^2|u_{n+1/2}|_3^2. \qquad (3.33)
\end{aligned}$$

Combine (3.28)–(3.33) to obtain

$$\Delta t\sum_{n=0}^{M-1}|Intp(u_n,p_n;\phi^h_{n+1/2})|$$
$$\leqslant \Delta tC\|\phi^h_{n+1}\|^2+(\varepsilon_1+\varepsilon_2+\varepsilon_3+\varepsilon_4)\Delta t\nu\|\nabla\phi^h_{n+1/2}\|^2$$
$$+C(\Delta t)^4(\|u_{ttt}\|^2_{2,0}+\nu^{-1}\|p_{tt}\|^2_{2,0}+\|f_{tt}\|^2_{2,0}+\nu\|\nabla u_{tt}\|^2_{2,0}$$
$$+\nu^{-1}\|\nabla u_{tt}\|^4_{4,0}+\nu^{-1}|||\nabla u|||^4_{4,0}+\nu^{-1}|||\nabla u_{1/2}|||^4_{4,0}). \quad (3.34)$$

Let $\varepsilon_1=\varepsilon_2=\varepsilon_3=\varepsilon_4=1/12$ and with (3.24)–(3.27), (3.34), from (3.23) we obtain

$$\|\phi^h_M\|^2+\nu\Delta t\sum_{n=0}^{M-1}\|\nabla\phi^h_{n+1/2}\|^2$$
$$\leqslant \Delta t\sum_{n=0}^{M-1}C(\nu^{-3}\|\nabla u_{n+1/2}\|^4+1)\|\phi^h_{n+1/2}\|^2+C\nu h^{2k}|||u|||^2_{2,k+1}$$
$$+C\nu^{-1}h^{2k+1}\left(|||u|||^4_{4,k+1}+|||\nabla u|||^4_{4,0}\right)$$
$$+C\nu^{-1}h^{2k}\left(|||u|||^4_{4,k+1}+\nu^{-1}(\|u^h_0\|^2+\nu^{-1}|||f|||^2_{2,*})\right)$$
$$+C\nu^{-1}h^{2s+2}|||p_{1/2}|||^2_{2,s+1}+C\nu^{-1}\alpha^4|||u|||^2_{4,1}|||u|||^2_{4,3}$$
$$+C(\Delta t)^4(\|u_{ttt}\|^2_{2,0}+\nu^{-1}\|p_{tt}\|^2_{2,0}+\|f_{tt}\|^2_{2,0}$$
$$+\nu\|\nabla u_{tt}\|^2_{2,0}+\nu^{-1}\|\nabla u_{tt}\|^4_{4,0}$$
$$+\nu^{-1}|||\nabla u|||^4_{4,0}+\nu^{-1}|||\nabla u_{1/2}|||^4_{4,0}). \quad (3.35)$$

Hence, with Δt sufficiently small, i.e. $\Delta t<C(\nu^{-3}|||\nabla u|||^4_{\infty,0}+1)^{-1}$, from Gronwall's Lemma (see Lemma 2.15), we have

$$\|\phi^h_M\|^2+\nu\Delta t\sum_{n=0}^{M-1}\|\nabla\phi^h_{n+1/2}\|^2$$
$$\leqslant C^*\Big\{\nu^{-1}h^{2k+1}\left(|||u|||^4_{4,k+1}+|||\nabla u|||^4_{4,0}\right)+\nu h^{2k}|||u|||^2_{2,k+1}$$
$$+\nu^{-1}h^{2k}\left(|||u|||^4_{4,k+1}+\nu^{-1}(\|u^h_0\|^2+\nu^{-1}|||f|||^2_{2,*})\right)+\nu^{-1}h^{2s+2}|||p_{1/2}|||^2_{2,s+1}$$
$$+C\nu^{-1}\alpha^4|||u|||^2_{4,1}|||u|||^2_{4,3}+(\Delta t)^4(\|u_{ttt}\|^2_{2,0}+\nu^{-1}\|p_{tt}\|^2_{2,0}+\|f_{tt}\|^2_{2,0}$$
$$+\nu\|\nabla u_{tt}\|^2_{2,0}+\nu^{-1}\|\nabla u_{tt}\|^4_{4,0}+\nu^{-1}|||\nabla u|||^4_{4,0}+\nu^{-1}|||\nabla u_{1/2}|||^4_{4,0})\Big\}, \quad (3.36)$$

where $C^*=C\exp(C\nu^{-3}T)$

Estimate (3.5) then follows from the triangle inequality and (3.36).

To obtain (3.6), we use (3.36) and

$$\|\nabla(u(t_{n+1/2})-(u^h_{n+1}+u^h_n)/2)\|^2$$
$$\leqslant\|\nabla(u(t_{n+1/2})-u_{n+1/2})\|^2+\|\nabla\eta_{n+1/2}\|^2+\|\nabla\phi^h_{n+1/2}\|^2$$
$$\leqslant\frac{(\Delta t)^3}{48}\int_{t_n}^{t_{n+1}}\|\nabla u_{tt}\|^2\,dt+Ch^{2k}|u_{n+1}|^2_{k+1}+Ch^{2k}|u_n|^2_{k+1}$$
$$+\|\nabla\phi^h_{n+1/2}\|^2. \quad \square \quad (3.37)$$

4. Numerical experiments

In this section, we present several numerical experiments to test the algorithms presented herein. Using the Green–Taylor vortex problem, we confirm the predicted convergence rates of the previous section, and also use it to compare accuracy of all the algorithms. Further testing is then performed using the flow over a step and around a cylinder benchmark problems. We use the software *FreeFem++* [26] to run the numerical tests.

The models are discretized with the full CN method, the nonlinear system was solved by a fixed point iteration of the form

$$b(\mathbf{u}^k_{n+1},\mathbf{v}^k_{n+1},\mathbf{w})=b(\mathbf{u}^{k-1}_{n+1},\mathbf{v}^k_{n+1},\mathbf{w}),$$

and discretized in space using the FEM with Taylor–Hood elements (continuous piecewise quadratic polynomials for the velocity and linears for the pressure). A multi-frontal Gauss LU factorization implemented in the package UMFPACK (provided with the FreeFem++ software) was used as our linear solver. Using the same method for both also allows a fair comparison of NS-α and NS-$\bar{\omega}$.

4.1. Convergence rate verification

Our first test is designed to test (and does confirm) the predicted rates of convergence. The problem of simulating decay of the Green–Taylor vortex, [22,54], is an interesting test problem in which the true solution is known. It was used as a numerical test in Chorin [10], Tafti [53] and John and Layton [30]. For a very insightful and detailed analysis of the problem for LES models see Barbato et al. [2] and Berselli [4]. The prescribed solution in $\Omega=(0,1)\times(0,1)$ has the form

$$u_1(x,y,t)=-\cos(n\pi x)\sin(n\pi y)e^{-2n^2\pi^2t/\tau},$$
$$u_2(x,y,t)=\sin(n\pi x)\cos(n\pi y)e^{-2n^2\pi^2t/\tau},$$
$$p(x,y,t)=-\frac{1}{4}(\cos(2n\pi x)+\cos(2n\pi y))e^{-2n^2\pi^2t/\tau}.$$

When the relaxation time $\tau=Re$, this is a solution of the NSE with $f=0$, consisting of an $n\times n$ array of oppositely signed vortices that decay as $t\to\infty$.

In our test, we choose $n=1$, $\Delta t=0.005$, $T=1$ and $\alpha=h=1/m$, where m is the number of subdivisions of the interval $(0,1)$. The results for the NS-$\bar{\omega}$ model are presented in Table 1. The convergence rate is calculated from the error at two successive values of h in the usual manner by postulating $e(h)=Ch^\beta$ and solving for β via $\beta=\ln(e(h_1)/e(h_2))/\ln(h_1/h_2)$.

From the table we see the convergence rate approaches the second order predicted for $|||\nabla u-\nabla u^h|||_{2,0}$. We also see what appears to be an L^2 lift for $|||u-u^h|||_{\infty,0}$.

4.2. Algorithm runtime comparison

The main motivation for computing with NS-$\bar{\omega}$ versus NS-α was for more efficiency, but not at the cost of less accuracy. In the next experiment, we compute the CN NS-α scheme (2.11) and (2.12) and the CN NS-$\bar{\omega}$ scheme (2.11) and (2.13) for the Chorin problem with the same parameters as used in the simulation presented in Table 1, and with $Re=100$. Shown in Table 2 are runtimes and in Tables 3,4 errors for both of these algorithms, as well as runtimes and errors for the CNLE and CNQE schemes for NS-$\bar{\omega}$ (as discussed above, such schemes are not possible for NS-α).

Table 1
Errors and convergence rates for NS-$\bar{\omega}$ at $Re=10^5$.

m	$\|\|\|u-u^h\|\|\|_{\infty,0}$	Rate	$\|\|\|\nabla u-\nabla u^h\|\|\|_{2,0}$	Rate
8	$1.3974\cdot10^{-1}$		5.03788	
16	$4.06505\cdot10^{-2}$	1.78	3.36582	0.58
24	$1.70328\cdot10^{-2}$	2.15	2.27963	0.96
32	$8.5897\cdot10^{-3}$	2.38	1.6152	1.19
40	$4.81706\cdot10^{-3}$	2.59	1.18214	1.40
48	$2.90948\cdot10^{-3}$	2.76	$8.85739\cdot10^{-1}$	1.58
56	$1.85706\cdot10^{-3}$	2.91	$6.76137\cdot10^{-1}$	1.75
64	$1.23504\cdot10^{-3}$	3.05	$5.24409\cdot10^{-1}$	1.90
72	$8.48737\cdot10^{-4}$	3.18	$4.12513\cdot10^{-1}$	2.04

Table 2
Run times of models at $Re = 100$.

m	NS $-\bar{\omega}$	NS $-\alpha$	NS $-\bar{\omega}$CNLE	NS $-\bar{\omega}$CQLE
4	25.45	89.85	13.86	14.06
8	89.06	278.41	49.80	50.687
16	361.27	1117.48	205.75	206.27
32	1509.67	4161.5	830.015	840.78
64	6883.17	22557.7	3787.27	3948.25

Table 3
The $|||u - u^h|||_{\infty,0}$ errors at $Re = 100$.

m	NS $-\bar{\omega}$	NS $-\alpha$	NS $-\bar{\omega}$CNLE	NS $-\bar{\omega}$CNQE
4	$5.5263 \cdot 10^{-2}$	$8.54457 \cdot 10^{-1}$	$5.53164 \cdot 10^{-2}$	$5.53156 \cdot 10^{-2}$
8	$7.68681 \cdot 10^{-3}$	$2.17741 \cdot 10^{-1}$	$7.69444 \cdot 10^{-3}$	$7.69427 \cdot 10^{-3}$
16	$1.52416 \cdot 10^{-3}$	$5.36912 \cdot 10^{-2}$	$1.52558 \cdot 10^{-3}$	$1.52553 \cdot 10^{-3}$
32	$2.19401 \cdot 10^{-4}$	$1.30726 \cdot 10^{-2}$	$2.19642 \cdot 10^{-4}$	$2.19637 \cdot 10^{-4}$
64	$2.39093 \cdot 10^{-5}$	$3.2016 \cdot 10^{-3}$	$2.39978 \cdot 10^{-5}$	$2.39979 \cdot 10^{-5}$

Table 2 shows, as expected, that the CN scheme for CN NS-$\bar{\omega}$ is significantly faster than that for NS-α. This is no surprise since it generates much smaller matrices and is stable in a stronger norm. It is more interesting that in Tables 3 and 4 we can observe that CN NS-$\bar{\omega}$ and two linearizations of it (CNLE and CNQE) are also much more accurate than the expensive NS-α scheme.

Remark 4.1. It appears from Tables 3 and 4 that the scheme used to compute NS-α has a reduced order of convergence compared to NS-$\bar{\omega}$. Convergence rates for CN implementations of NS-α is under study in [11].

4.3. Flow around a cylinder

Our next numerical illustration is for two-dimensional under-resolved flow around a cylinder. This is a well known benchmark problem taken from Schäfer and Turek [49]. A detailed numerical study of this problem for the NSE is done by John in [29]. This fluid flow problem is not turbulent but does have interesting features. The flow patterns are driven by interaction of a fluid with a wall. Such flows are critical if regularizations (and LES models also) are to be useful for real, industrial type flows. It is also interesting since success and failure are clear (vortex street or not) and thus comparison of higher order statistics is not necessary to reach a clear conclusion. We note that it is known that many LES models have difficulties with flows involving interactions with walls and with flows near points of transition from one flow regime to another. Thus, this simple flow is actually quite difficult to simulate successfully by an (under-resolved) model with strong enough regularization to handle higher Reynolds number problems.

The time dependent inflow and outflow profile are

$$u_1(0,y,t) = u_1(2.2,y,t) = \frac{6}{0.41^2}\sin(\pi t/8)y(0.41-y),$$
$$u_2(0,y,t) = u_2(2.2,y,t) = 0.$$

No slip boundary conditions are prescribed along the top and bottom walls and the initial condition is $u(x,y,0) = 0$. The viscosity is $\nu = 10^{-3}$ and the external force $f = 0$. The Reynolds number of the flow, based on the diameter of the cylinder and on the mean velocity inflow is $0 \leqslant Re \leqslant 100$. FreeFem provides 3 meshes for testing this problem, the finest of which is able to resolve the problem for the Navier–Stokes equations. These are shown in Fig. 1. The filtering radius α is chosen to be the average element length of the

Table 4
The $|||\nabla u - \nabla u^h|||_{2,0}$ errors at $Re = 10^2$.

m	NS $-\bar{\omega}$	NS $-\alpha$	NS $-\bar{\omega}$CNLE	NS $-\bar{\omega}$CQLE
4	1.10152	7.30353	1.10395	1.1039
8	$2.97759 \cdot 10^{-1}$	2.13637	$2.98372 \cdot 10^{-1}$	$2.98329 \cdot 10^{-1}$
16	$5.32635 \cdot 10^{-2}$	$6.86788 \cdot 10^{-1}$	$5.33942 \cdot 10^{-2}$	$5.33945 \cdot 10^{-2}$
32	$8.18802 \cdot 10^{-3}$	$2.31259 \cdot 10^{-1}$	$8.2195 \cdot 10^{-3}$	$8.24665 \cdot 10^{-3}$
64	$1.22089 \cdot 10^{-3}$	$7.97553 \cdot 10^{-2}$	$1.2308 \cdot 10^{-3}$	$1.24955 \cdot 10^{-3}$

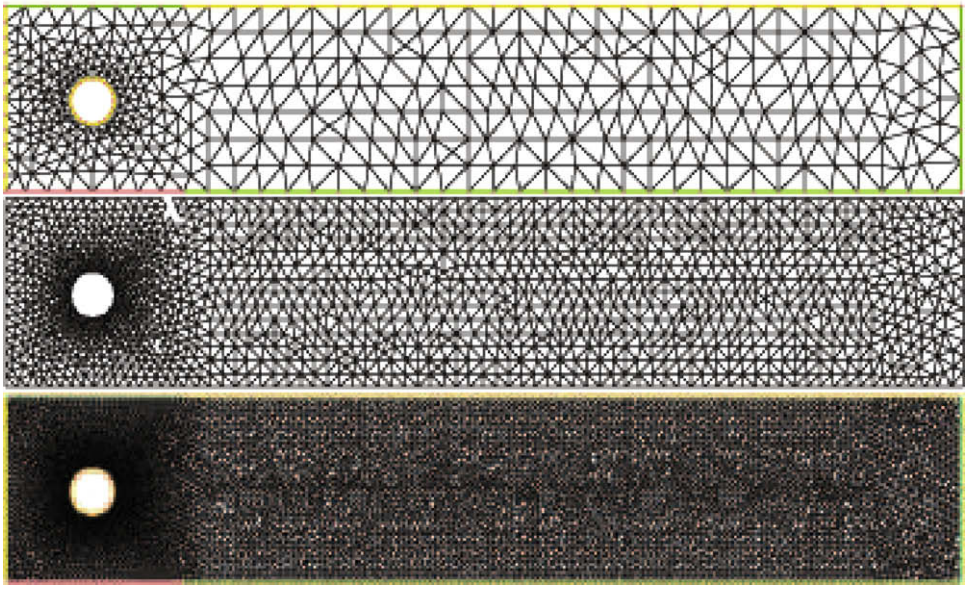

Fig. 1. Shown below are three levels of mesh refinement provided by FreeFem for computing flow around a cylinder. The meshes provide, respectively, 3975, 14,455, and 56,702 degrees of freedom for the computations.

respective mesh. There is discussion in the LES community concerning the coupling of the averaging radius (here α) and the mesh-width h. Analysis sometimes points to $\alpha \gg O(h)$ (e.g., $\alpha \simeq \sqrt{h}$) while the needs of practical computing often force $\alpha \simeq h$ and even varying α according to the local mesh-width. We have selected $\alpha = h$ in our tests (the length of the cylinder divided by the number of mesh points around the cylinder).

Picture of the flow field for this problem can be found in [29] and it shows the development of vortices behind the cylinder. For this setting, it is expected that, as the flow increases, from time $t = 2$ to $t = 4$, two vortices start to develop behind the cylinder. Between $t = 4$ and $t = 5$, the vortices should separate from the cylinder, so that a vortex street develops, and they continue to be visible through the final time $t = 8$. This can be also seen in Fig. 2, which is the solution for resolved Navier–Stokes equations on mesh 3.

However, we were unable to obtain exactly these results for NS-α or NS-$\bar{\omega}$ on coarser meshes. On the finest mesh, mesh 3, upon which the NSE is fully resolved NSE and NS-$\bar{\omega}$ were comparable and successful. The figures are omitted since a mesh fine enough for the NSE to give good results is not the interesting case. Regularizations often give approximate solutions that look like NSE solutions at lower Reynolds numbers (rather than restrictions of the fine mesh solutions to coarser meshes). Some of this behavior is observed for the NS-α and NS-$\bar{\omega}$ on the coarser meshes. For NS-α, we were only able to get results for mesh 1, because we were unable to make the nonlinear iteration converge for the finer meshes. The failure modes of NS-α are thus a large over-damping and failure to predict a vortex street on mesh 1 and convergence failure of accepted and robust iterative solvers on mesh 2. This convergence failure is likely a technical feature of NS-α requiring an adapted solver, and is under study. The flow resulting from NS-α on mesh 1 at time $t = 8$ is shown in Fig. 4, and does not capture the correct flow dynamics. Mesh 2 results for NS-$\bar{\omega}$ are presented for $t = 8$ in Fig. 3, and it can be seen that it was also unable to capture the correct flow behavior; it has the general outline of the flow correct and predicts a vortex street but the wake is over-damped significantly.

We believe understanding the limitations of a model are just as important (if not more so) as knowing what it does well. Indeed, the failure of the models to accurately predict the vortex street

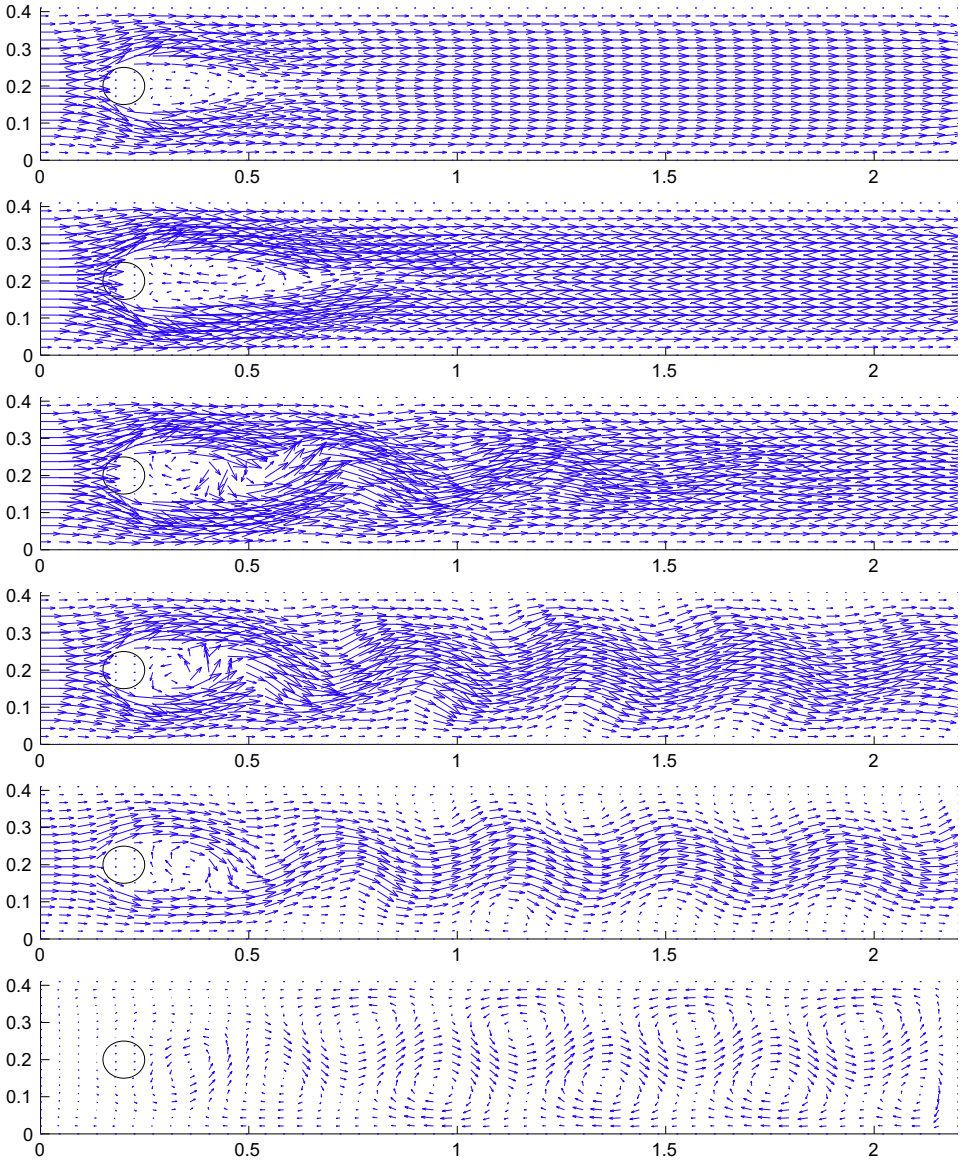

Fig. 2. NSE (rotation form) solved on finest mesh, timestep $\Delta t = 0.005$, shown at times 2, 4, 5, 6, 7, 8. The vortex street is formed by $t = 8$.

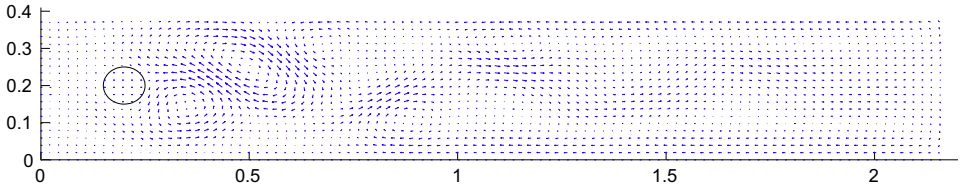

Fig. 3. NS-$\bar{\omega}$ model computed on mesh 2 at time $t = 8$, $\Delta t = 0.005$, $\alpha = 0.0025\pi$, vortex street appears but is over-damped.

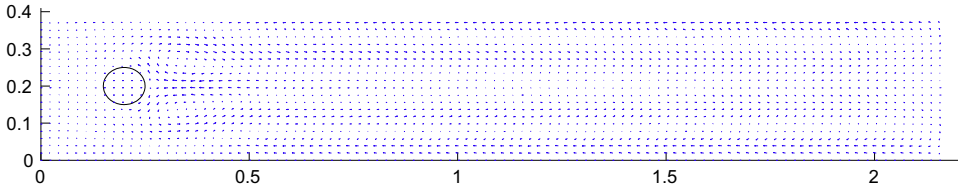

Fig. 4. NS-α model computed on mesh 1 at time $t = 8$, $\Delta t = 0.005$, $\alpha = 0.005\pi$, no vortex street forms.

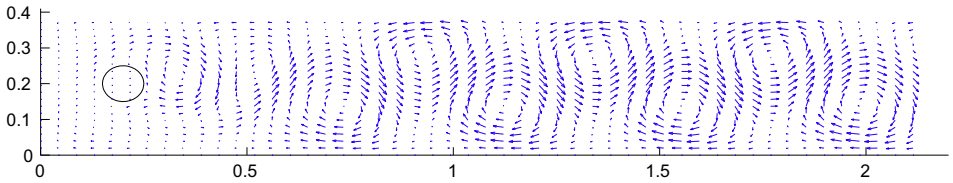

Fig. 5. NS-$\bar{\omega}$ model with grad–div stabilization (with parameter $\gamma = 1$) computed on mesh 2 at time $t = 8$, $\Delta t = 0.005$, $\alpha = 0.0025\pi$. Here the vortex street is accurately predicted; without grad–div stabilization the test fails, Fig. 3.

on the coarse meshes led to a deeper investigation which provided both an explanation of the failure as well as a method to fix it. As is discussed in Section 1.4, the rotational form of the nonlinearity (which these models use) can lead to numerical inaccuracies. However, these inaccuracies can often be "fixed" by using grad–div stabilization. Indeed by adding the term $(\nabla \cdot u^h, \nabla \cdot v^h)$, the model gives accurate results, Fig. 5. Note that a parameter $\gamma > 0$ is often associated with the grad–div stabilization term as $\gamma(\nabla \cdot u^h, \nabla \cdot v^h)$. For computations using Taylor–Hood elements, which are employed in our experiments, it was shown in [6] that γ needs to be chosen of order 1 to be effective. However, the parameter γ can still be slightly varied to improve results. For the flow around a cylinder experiment with grad–div stabilization, we found no choice of γ gave better results than $\gamma = 1$. For the last numerical experiment, flow over a step, the choice of $\gamma = 0.5$ was optimal.

4.4. Numerical experiments for 2D step problem

Our final experiment is to test the models on the 2D full step benchmark problem, to see if the model retards separation of vortices behind a blunt body, near the critical Reynolds number. To do so, we study the flow across a full step in 2D. A discussion of this test problem can be found in Gunzburger [18] and John and Liakos [31]. The most distinctive feature of this flow is a recirculating vortex behind the step that detaches in the range $500 \leqslant Re \leqslant 700$. This is illustrated in Fig. 6, which represents the true solution (i.e. NSE on fine mesh). We study the flow for $\nu = 1/600$, when eddies are known to shed, for NS-$\bar{\omega}$, and NS-$\bar{\omega}$ with grad–div stabilization. As with the flow around a cylinder experiment, we were unable to run NS-α (on any of the meshes) to completion due to problems converging the nonlinear iteration.

The domain of the two-dimensional flow across a step is displayed in Fig. 7. We present results for a parabolic inflow profile, which is given by $u = (u_1, u_2)^T$, with $u_1 = y(10 - y)/25$, $u_2 = 0$. No-slip boundary condition is prescribed on the top and bottom boundary as well as on the step. At the outflow we imposed the "do nothing" boundary condition.

The computations were performed on various grids with the software FreeFem++ [26]. The grid level 3 is the finest with the number of degrees of freedom being 41,475. Then the grid level 2 and 1 are coarser with the number of degrees of freedom 24,580 and 5836, respectively. For the fully resolved NSE simulation, which is our "truth" solution, we used a fine grid (level 3) whereas a much coarser grid (levels 2 and 1) was used for testing the models. The point is to compare the performance of the various options in underresolved simulations by comparison against a "truth"/fully-resolved solution, Fig. 6.

The models were discretized in space with the Taylor–Hood finite-element. A fixed point iteration is applied to the nonlinear term. The averaging radius α depends on the mesh width and it is precisely stated below the figure of the simulation. The time step is $\Delta t = 0.005$.

We find that the NS-$\bar{\omega}$ simulation fails to predict vortex shedding on mesh 2, even with the grad–div stabilization but NS-$\bar{\omega}$ with a higher order of deconvolution $N = 1$ improves the shedding of the eddies. Similar results were found for the Leray-α model in [36], where it was suggested a lack of accuracy was to blame for such poor behavior. There, the addition of van Cittert approximate deconvolution was used to significantly improve the results. We discuss this modeling technique, and some preliminary numerical results using it in the next section.

Regarding the outflow condition, the "do nothing" outflow condition for the NS-$\bar{\omega}$ with grad–div stabilization in the numerical tests is not transparent. Numerical artifacts are seen near the outflow boundary. Therefore, for practical purposes one has to use a domain which is sufficiently large such that the boundary condi-

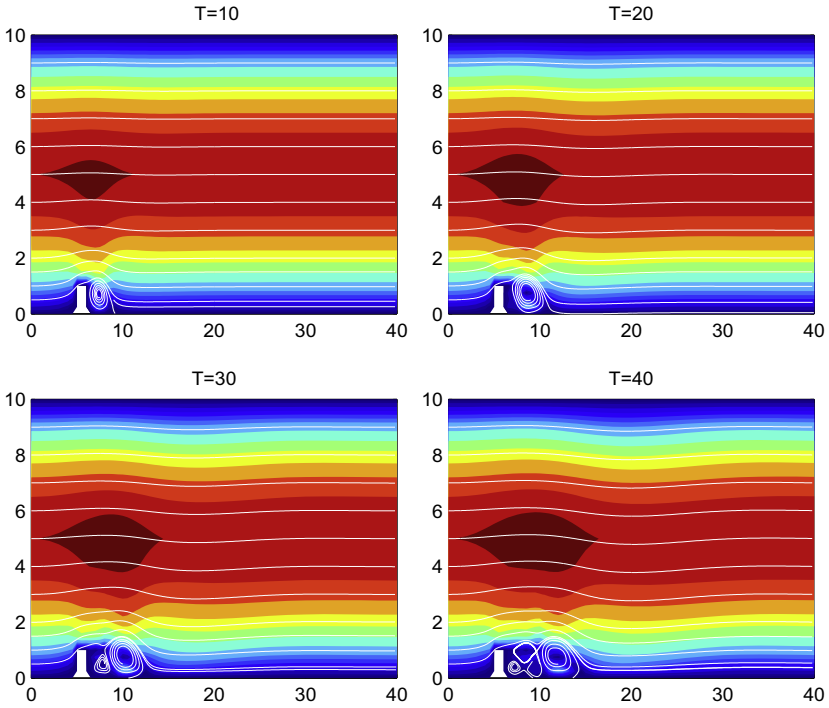

Fig. 6. NSE at $\nu = 1/600$, level 3 mesh.

tion is applied far enough from region of interest. This was also reported for the rotational form of the Navier–Stokes equations for 2D step simulation, [LMNOR08]. It is also known that the "do nothing" outflow boundary condition for the Poiseuille flow leads to incorrect computational results if the deformation tensor form of the viscous term is used or if the skew-symmetric form of the convective term is applied, [HRT96, J03].

5. Conclusions and future directions

Reduced models of fluid motion exist as intermediate steps in under-resolved flow simulations. Thus, within any approach to flow modeling the pairing of efficient algorithms with interesting models must be considered as part of the solution process going from fluid phenomena to numerical simulation. Considering possible combinations leads to interesting developments in continuum models as well as algorithms. We have considered one such development herein. The form of (1.1)–(1.3), its integral invariants, and its development from the deconvolution and NS-α circle of ideas suggest some possibilities for future progress. In addition, to grad–div stabilization, three natural ones are synthesis of NS alpha and NS-$\bar{\omega}$ models, higher accuracy in modeling through deconvolution and enhanced scale truncation through combination with VMM/ time relaxation ideas.

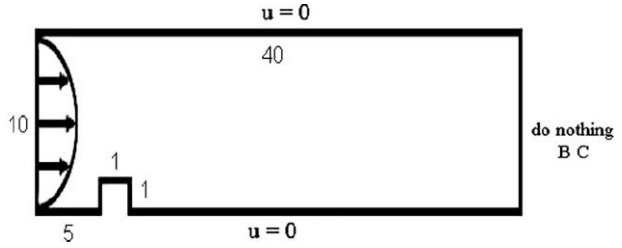

Fig. 7. Domain of the flow across a step.

Synthesis of NS-α and $\bar{\omega}$ models. Although our intuition is the contrary, further study of (1.1)–(1.3) and (1.4)–(1.6) could indicate that they perform well in different flow regions. If this is the case it might be valuable to study combinations and self-adaptive local transition between the models. A simple combination, preserving attractive theoretical properties is given by

$$u_t - \bar{u} \times (\nabla \times \bar{u}) + \nabla q - \nu \Delta u = f, \tag{5.1}$$

$$\nabla \cdot \bar{u} = 0, \quad \text{and} \quad -\alpha^2 \Delta \bar{u} + \bar{u} = u. \tag{5.2}$$

An interesting possibility is to include a switching parameter[2], $0 \leqslant \theta(x,t) \leqslant 1$, and consider

$$u_t - [\theta\bar{u} + (1-\theta)u] \times (\nabla \times [(1-\theta)\bar{u} + \theta u]) + \nabla q - \nu \Delta u = f, \tag{5.3}$$

$$\nabla \cdot [\theta\bar{u} + (1-\theta)u] = 0, \quad \text{and} \quad -\alpha^2 \Delta \bar{u} + \bar{u} = u. \tag{5.4}$$

This possibility must include determination of a method for self-adaptively switching between models locally, i.e., determining θ.

The NS-$\bar{\omega}$-deconvolution models. Computational experience of many years in CFD affirms that accuracy is still important. Two difficulties with (1.1)–(1.3) and (1.4)–(1.6) are that (i) low model accuracy of only $O(\alpha^2)$, and (ii) the differential/Hemholtz filter (1.3) does not truncate small scales effectively enough. One solution to both difficulties (following its success in the Leray-deconvolution models [37] is to study NS-$\bar{\omega}$-deconvolution models. To avoid extra notation, we give the first nontrivial example.

CNLE uses linear time extrapolation: $u(t_{n+1}) = 2u(t_n) - u(t_{n-1}) + O(\Delta t^2)$. A similar extrapolation can be used in scale space as a deconvolution operator: $u = 2\bar{\bar{u}} - \bar{u} + O(\alpha^4)$. Calling $D_1\bar{u} := 2\bar{\bar{u}} - \bar{u}$ it is a remarkable fact that not only does $D_1\bar{u}$ approximate u to higher order but it also truncates small scales much more effectively than $\bar{u}$, e.g., [37]. The NS-$\bar{\omega}$-deconvolution models are then (with D denoting the deconvolution operator)

$$u_t - u \times (\nabla \times D\bar{u}) + \nabla q - \nu \Delta u = f, \tag{5.5}$$

$$\nabla \cdot u = 0, \quad \text{and} \quad -\alpha^2 \Delta \bar{u} + \bar{u} = u, \tag{5.6}$$

[2] Included in a way to open the possibility of a robust mathematical theory.

and CNLE algorithms preserve their attractive properties for the entire family of deconvolution regularizations: with $U^n := \frac{3}{2}u^n - \frac{1}{2}u^{n-1}$

$$\frac{u^{n+1}-u^n}{\Delta t} - u^{n+\frac{1}{2}} \times (\nabla \times (D\overline{U^n})) - \nu\Delta u^{n+\frac{1}{2}} + \nabla p^{n+\frac{1}{2}} = f^{n+\frac{1}{2}},$$
$$\text{and} \quad \nabla \cdot u^{n+\frac{1}{2}} = 0. \tag{5.7}$$

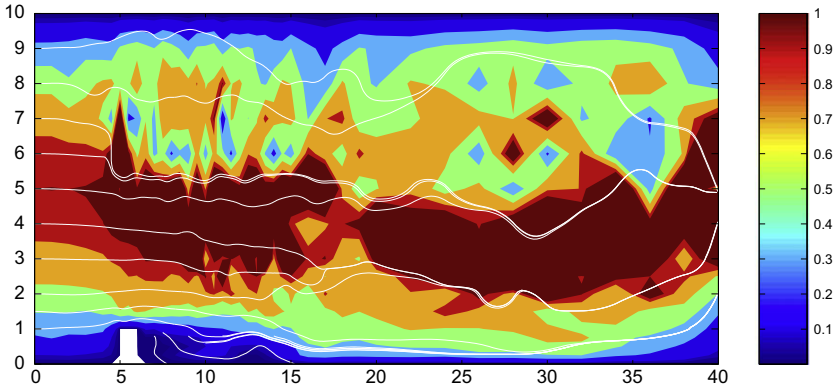

Fig. 8. NS-$\bar{\omega}$ at $T = 40$, $\nu = 1/600$, $\alpha = 0.125$ and level 2 grid.

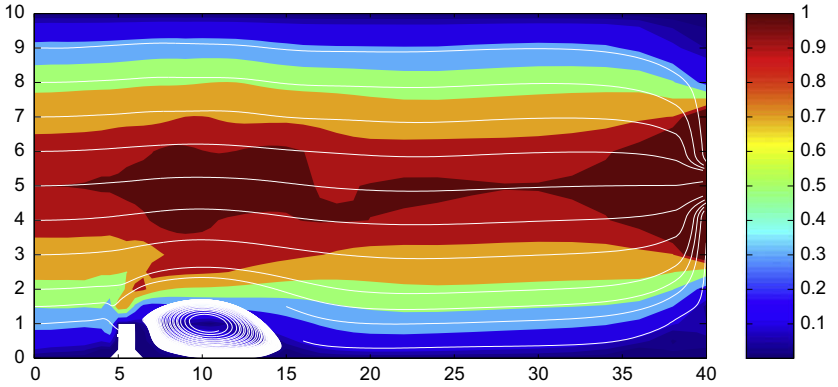

Fig. 9. NS-$\bar{\omega}$ with grad–div stabilization added (with parameter $\gamma = 0.5$), at $T = 40$, $\nu = 1/600$, $\alpha = 0.125$ and level 2 grid.

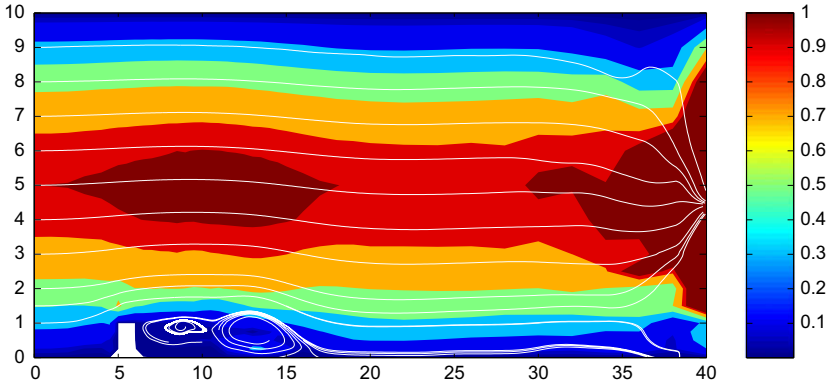

Fig. 10. NS-$\bar{\omega}$ with grad–div stabilization (with parameter $\gamma = 0.5$) and first order deconvolution, at $T = 40$, $\nu = 1/600$, $\alpha = 0.25$ and level 1 grid.

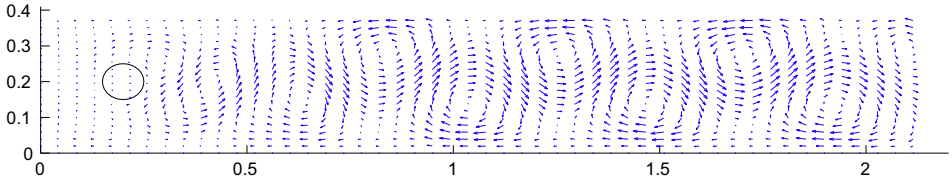

Fig. 11. NS-$\bar{\omega}$-deconvolution (N=1) model with grad–div stabilization (with parameter $\gamma = 0.5$), computed on mesh 1 at time $t = 8$, Δt=0.005, $\alpha = 0.005\pi$. Here the vortex street is accurately predicted.

The deconvolution operator involves repeated filtering. Efficiency is preserved if, as here, it acts on a velocity known from previous time levels (see Figs. 8,9).

We have done preliminary testing of the $N = 1$ NS-$\bar{\omega}$-deconvolution model for both the flow around a cylinder and over a step benchmark problems. Although on its own, modest improvement is made over NS-$\bar{\omega}$ testing, we have found remarkable results using the combination of first order deconvolution and grad–div stabilization. The results for the level 1 (coarsest) meshes are shown in Figs. 10 and 11. This combination clearly deserves future study, as in both cases an accurate prediction is made on the coarsest mesh.

Scale truncation, Eddy viscosity, VMMs and time relaxation. One basic difficulty shared by (1.1)–(1.3) and (1.4)–(1.6), e.g., [15,40], is that scale truncation is insufficient. While the model's microscales, η_{model}, (as predicted by turbulence phenomenology) is larger that the NSE microscale, η_{NSE}, it is far larger than the filter length scale:

$$\text{for } (1.1)\text{–}(1.3) \quad \text{and} \quad (1.4)\text{–}(1.6): \ \eta_{\text{model}} \gg \alpha \simeq O(h).$$

In the usual K41 phenomenology, [13], microscales can only be altered by increasing energy dissipation. There are three possibilities (the last two have less influence on the resolved scales) which can be added to any model to enhance scale truncation: (i) use algorithms which include extra numerical dissipation (which if not carefully done acts on all scales), (ii) subgrid Eddy viscosity/Variational Multiscale small–small Smagorinsky, [24,25], and (iii) time relaxation, e.g., [38,50–52]. Both models studied showed evidence of overdamping without any added dissipation. Thus, any added dissipation should be focused on the smallest resolved scale. We believe that VMMs and time relaxation are related and are fundamental tools for effective simulation of under-resolved flows because they do exactly this.

References

[1] G. Baker, Galerkin Approximation for the Navier–Stokes Equations, Report, Harvard University, 1976.
[2] D. Barbato, L.C. Berselli, C.R. Grisanti, Analytical and numerical results for the rational large Eddy simulation model, J. Math. Fluid Mech. 9 (2007) 44–74.
[3] Y. Bazilevs, V.M. Calo, J.A. Cottrell, T.J.R. Hughes, A. Reali, G. Sco- vazzi, Variational multiscale residual based turbulence modeling for large Eddy simulation of incompressible flows, Comput. Methods Appl. Mech. Engrg. 197 (2007) 173201.
[4] L.C. Berselli, On the large Eddy simulation of the Taylor–Green vortex, J. Math. Fluid Mech. 7 (2005) S164–S191.
[5] L.C. Berselli, T. Iliescu, W. Layton, Mathematics of Large Eddy Simulation of Turbulent Flows, Springer, Berlin, 2006.
[6] M. Braack, E. Burman, V. John, G. Lube, Stabilized finite element methods for the generalized Oseen problem, Comput. Methods Appl. Mech. Engrg. 196 (2007) 853–866.
[7] S. Brenner, L.R. Scott, The Mathematical Theory of Finite Element Methods, Springer-Verlag, 1994.
[8] A. Caglar, A Finite Element Approximation of the Navier–Stokes-Alpha Model, PIMS Preprint Series, PIMS-03-14, 2003.
[9] A. Cheskidov, D.D. Holm, E. Olson, E.S. Titi, On a Leray-α model of turbulence, Roy. Soc. Lon., Proc., Ser. A, Math., Phys. Engrg. Sci. 461 (2005) 629–649.
[10] A.J. Chorin, Numerical solution for the Navier–Stokes equations, Math. Comput. 22 (1968) 745–762.
[11] J. Connors, Convergence analysis and computational testing of a finite element discretization of the Navier–Stokes alpha model, Technical Report, University of Pittsburgh, 2008.
[12] V.V.Chepyzhov, E.S. Titi, M.I. Vishik, On the convergence of the Leray-α model to the trajectory attractor of the 3d Navier–Stokes system, Report, 2005.
[13] U. Frisch, Turbulence, Cambridge, 1995.
[14] C. Foias, D. Holm, E. Titi, The three dimensional viscous Camassa–Holm equations, and their relation to the Navier–Stokes equations and turbulence theory, J. Dyn. Diff. Eq. 14 (2002) 1–35.
[15] C. Foias, D. Holm, E. Titi, The Navier–Stokes-alpha model of fluid turbulence, Physica D (2001) 505–519.
[16] M. Germano, Differential filters for the large Eddy numerical simulation of turbulent flows, Phys. Fluids 29 (1986) 1755–1757.
[17] M. Germano, Differential filters of elliptic type, Phys. Fluids 29 (1986) 1757–1758.
[18] M.D. Gunzburger, Finite Element Methods for Viscous Incompressible Flows – A Guide to Theory, Practices, and Algorithms, Academic Press, 1989.
[19] B.J. Geurts, D.D. Holm, Leray and LANS-alpha modeling of turbulent mixing, J. Turbul. 7 (2006) 1–33.
[20] B.J. Geurts, D.D. Holm, Regularization modeling for large Eddy simulation, Phys. Fluids 15 (2003).
[21] G.P. Galdi, W.J. Layton, Approximation of the large Eddy in fluid motion II: A model for space-filtered flow, Math. Models Methods Appl. Sci. 10 (2000) 343–350.
[22] A.E. Green, G.I. Taylor, Mechanism of the production of small eddies from larger ones, Proc. Roy. Soc. A 158 (1937) 499–521.
[23] J.L. Guermond, S. Prudhomme, J.T. Oden, An interpretation of the NS alpha model as a frame indifferent Leray regularization, Phys. D Nonlinear Phenom. 177 (2003) 23–30.
[24] T. Hughes, L. Mazzei, K. Jansen, Large Eddy simulation and the variational multiscale method, Comput. Visual. Sci. 3 (1/2) (2000) 47–59.
[25] T. Hughes, A. Oberai, L. Mazzei, Large Eddy simulation of turbulent channel flows by the variational multiscale method, Phys. Fluids 13 (6) (2001) 1784–1799.
[26] F. Hecht, O. Pironneau, FreeFem++ webpage: <http://www.freefem.org>.
[27] J.G. Heywood, R. Rannacher, Finite element approximation of the nonstationary Navier–Stokes problem, Part IV: Error analysis for the second order time discretization, SIAM J. Numer. Anal. 2 (1990) 353–384.
[28] A.A. Ilyin, E.M. Lunasin, E.S. Titi, A modified Leray-α subgrid-scale model of turbulence, Report, 2005.
[29] V. John, Reference values for drag and lift of a two dimensional time dependent flow around a cylinder, Int. J. Numer. Meth. Fluids 44 (2004) 777–788.
[30] V. John, W. Layton, Analysis of numerical errors in large Eddy simulation, SIAM J. Numer. Anal. 40 (2002) 995–1020.
[31] V. John, A. Liakos, Time dependent flow across a step: the slip with friction boundary condition, Int. J. Numer. Meth. Fluids 50 (2006) 713–731.
[32] J.J. Koenderink, The structure of images, Biol. Cybernet. 50 (1984) 363–370.
[33] J. Leray, Essay sur les mouvements plans d'une liquide visqueux que limitent des parois, J. Math. Pur. Appl., Paris Ser. IX 13 (1934) 331–418.
[34] J. Leray, Sur les mouvements d'une liquide visqueux emplissant l'espace, Acta Math. 63 (1934) 193–248.
[35] W. Layton, C. Manica, M. Neda, M. Olshanskii, L. Rebholz, On the accuracy of the rotation form in simulations of the Navier–Stokes equations, J. Comput. Phys., in press. Preprint available at: <http://www.mathematics.pitt.edu/research/technical-reports.php>.
[36] W. Layton, C. Manica, M. Neda, L. Rebholz, The joint Helicity–Energy cascade for homogeneous, isotropic turbulence generated by approximate deconvolution models, Adv. Appl. Fluid Mech. 4 (1) (2008) 1–46.
[37] W. Layton, C. Manica, M. Neda, L. Rebholz, Numerical analysis and computational testing of a high accuracy Leray-deconvolution model of turbulence, Numer. Methods Diff. Eq. 24 (2) (2008) 555–582.
[38] W. Layton, M. Neda, Truncation of scales by time relaxation, J. Math. Anal. Appl. 325 (2) (2007) 788–807.
[39] G. Lube, M. Olshanskii, Stable finite element calculations of incompressible flows using the rotation form of convection, IMA J. Numer. Anal. 22 (2002) 437–461.
[40] W. Layton, I. Stanculescu, C. Trenchea, Theory of the NS-$\bar{\omega}$ model, Technical Report, University of Pittsburgh, 2008.
[41] T. Lindeberg, Scale-Space Theory in Computer Vision, Kluwer, Dordrecht, 1994.
[42] C. Manica, S. Kaya Merdan, Convergence analysis of the finite element method for a fundamental model in turbulence, Technical Report, University of Pittsburgh, 2006.
[43] H. Moffatt, A. Tsoniber, Helicity in laminar and turbulent flow, Ann. Rev. Fluid Mech. 24 (1992) 281–312.
[44] M. Olshanskii, A low order Galerkin nite element method for the Navier–Stokes equations of steady incompressible ow: a stabilization issue and iterative methods, Comput. Meth. Appl. Mech. Engrg. 191 (2002) 5515–5536.
[45] M. Olshanski, A. Reusken, Navier–Stokes equations in rotation form: a robust multigrid solver for the velocity problem, SIAM J. Sci. Comput. 23 (2002) 1682–1706.
[46] M. Olshanski, A. Reusken, Grad–div stabilization for Stokes equations, Math. Comput. 73 (248) (2004) 1699–1718.
[47] L. Rebholz, Conservation laws of turbulence models, J. Math. Anal. Appl. 326 (1) (2007) 33–45.
[48] P. Saugat, Large Eddy Simulation for Incompressible Flows, Springer-Verlag, Berlin, 2001.
[49] M. Schäfer, S. Turek, Benchmark computations of laminar flow around cylinder, Flow Simulation with High-Performance Computers, vol. 2, Vieweg, 1996.
[50] S. Stolz, N.A. Adams, On the approximate deconvolution procedure for LES, Phys. Fluids 2 (1999) 1699–1701.
[51] S. Stolz, N.A. Adams, L. Kleiser, The approximate deconvolution model for LES of compressible flows and its application to shock-turbulent-boundary-layer interaction, Phys. Fluids 13 (2001) 2985.
[52] S. Stolz, N.A. Adams, L. Kleiser, An approximate deconvolution model for large Eddy simulation with application to wall-bounded flows, Phys. Fluids 13 (2001) 997.
[53] D. Tafti, Comparison of some upwind-biased high-order formulations with a second order central-difference scheme for time integration of the incompressible Navier–Stokes equations, Comput. Fluids 25 (1996) 647–665.
[54] G.I. Taylor, On decay of vortices in a viscous fluid, Phil. Mag. 46 (1923) 671–674.
[55] E. Zeidler, Applied Functional Analysis: Applications to Mathematical Physics, Springer-Verlag, New York, 1995.